

Simulations and Experiments of Magnetic and Mechanical Effects in Magneto-Motive Ultrasound Imaging

Esayas Atile

June 11, 2013



LUND UNIVERSITY

Master's Thesis

Faculty of Engineering, LTH
Department of Measurement Technology and
Industrial Electrical Engineering
Division of Electrical Measurements

Supervisors: Tomas Jansson, Maria Evertsson

Abstract

Superparamagnetic nanoparticles have been used for different applications, especially for MRI as a contrast agent. Recently, a new technique called Magneto-motive ultrasound (MMUS) imaging was introduced making these particles also work for as a contrast agent for ultrasound. This method uses a time varying magnetic field as an excitation source to provoke motion of magnetic nanoparticles laden in for instance a tissue mimicking phantom. Ultrasound is then used to detect and image the motion. In this project both experimentation and simulation have been performed to show that motions induced outside nanoparticle laden regions are a result of mechanical wave motion. Various concentrations inside a tissue mimicking phantom have been modeled.

As the results from the experimental and simulation show, there is a correspondence between the experimental and the simulation results. The triggered motion by the magnetic field makes the magnetic inserts to displace and thereby the surrounding motion, in all directions. However, ultrasound detects only the z-component movement. Considering the z-component displacement of the magnetic inserts and the area in between, in both the experimental and the simulation results, both the inserts and the area in between happen to displace with different amplitudes and with a π -radian phase shift. This suggests that, there is a clear contrast between the magnetic nanoparticles and the surrounding where the inserts are labeled. This helps to differentiate the magnetic inserts from the surrounding where the inserts are embedded by considering the phase shift.

Acknowledgements

I would like to express my deepest gratitude to my supervisors, Tomas Jansson and Maria Evertsson for their uninterrupted support and guidance throughout this project. They both were very patient and understanding, without their supervision this project wouldn't be real. It is such a great honor to have worked with you both, and I thank you for that. A special thanks to Per, who never hesitated to help me with all the questions I had. His valuable comments and wonderful discussions were very helpful. Thank you, Ingrid, for your great help and valuable comments, which helped me finish the project at the end.

Thank you, Axel, for your helpful comments and warm welcoming. I would like to Thank Mikael, who I have had helpful discussions with. Thank you, Magnus, for your great support and comments; it was such a pleasure working with you. Thank you, Fredrik, for your great assistance with the computer. Thank you, Désirée, for your great help and cooperation. I would also like to thank the people in the department and also everyone in the Ultrasound group, who I have had great time with. Last but not least, I would like to thank my brother Alebachew, who I grew up looking up to him, for his financial and moral support.

Contents

Abstract	2
Acknowledgements	3
1, Introduction	6
2, Background Theory	8
2.1 Physics of ultrasound.....	8
2.1.1 Wave propagation.....	8
2.1.2 Modes of propagation.....	9
2.1.3 Wavelength, frequency and speed	10
2.2 Magnetic field	12
2.3 Magnetic susceptibility.....	14
2.4 Magnetic nanoparticles.....	15
2.5 Magnetic force and energy	17
2.6 Magnetic Force acting on magnetic nanoparticles	18
2.7 Motion of Magnetic nanoparticles.....	22
2.8 Tissue magnetic field interaction	23
2.9 Tissue ultrasound interaction.....	24
2.10 Contrast agents used in ultrasound imaging.....	26
3, Materials and Methods	29
3.1 Experimentation	29
3.1.1 The nanoparticles	29
3.1.2 Preparation of tissue mimicking Phantoms	29
3.1.3 Experimental set up.....	30
3.2 Simulations.....	31
3.2.1 Description of Comsol Program and its use in this project	32
3.2.2 Simulation procedures	33

4, Results	39
4.1 Experimental results	39
4.1.1 Experimental results from the high concentration set- up	39
4.1.2 Experimental results from the low concentration set up	44
4.2 Simulation results	49
4.2.1 2D-Axis-symmetric Simulation results	49
4.2.2 3D-simulation results using a 4Hz excitation frequency.....	51
4.2.3 3D-simulation results using a 8Hz excitation frequency.....	58
5, Discussions	61
5.1 Experimental results	61
5.2 Simulation results of MMUS imaging	64
5.2.1 2D-axis symmetric	64
5.2.2 3D-with an excitation frequency of 4Hz	65
5.2.3 3D with an excitation frequency of 8Hz.....	67
6, Conclusions	69
7, References	70

1, Introduction

Ultrasound is a sound energy that travels in the form of waves and has a frequency greater than the upper limit of a human hearing range, 20 kHz [1]. It is this sound energy, which has been implemented for different applications especially quite often for medical diagnostics. Nowadays, in the medical field, this technique becomes one of the most widely used imaging modalities, due to its being cost effective, real time, and non-ionizing. However, ultrasound has also limitations; it has limited resolutions and contrast, though still high frequency ultrasound in general achieves better resolutions than magnetic resonance imaging (MRI). Imaging deeper regions could also be possible with ultrasound, but still with reasonable resolution and this limits ultrasound not to image events at the cellular and molecular level, which is due to lack of contrast. Research has been conducted to improve the ultrasound images and also to be able to image events at a molecular level with reasonable resolutions. The introduction of contrast agents has changed a lot of things and brought a big change in ultrasound images and also believed that it paved the way for the modern contrast agents, though new researches are still underway. The most commonly used ultrasound contrast agent is Micro bubbles, their scattering properties of these gas bubbles in response to the ultrasonic field have made them very desirable in ultrasound diagnostic. Even though this ultrasound agent has a very good scattering property, it has limited use in molecular imaging technique. This is because these agents are very unstable and have short half life in the circulatory system and may collapse when exposed to high frequency sound pressure [2]. Besides improving the contrast of ultrasound images, there is this thought that the contrast agent can give additional information about the tissue in which they are embedded in, but unfortunately none of the common ultrasound contrast agent manages to do that.

However, nowadays, because of their size, nanoparticles are in use for different purposes. Magnetic nanoparticle contrast agents are being extensively used to image events at molecular levels. These agents have been used for MRI for over a decade now. It has been tried to use these

agents for ultrasound imaging, but because of their being small sized, less reflectivity and inefficiency of ultrasound limited resolution and contrast, it has become difficult to detect them directly. So this is where the new technique called Magneto-motive Ultrasound (MMUS) Imaging is introduced. For the first time this technique was introduced and used by M. Mehrmohammadi [3]. Magneto-motive ultrasound imaging uses a highly focused time varying magnetic field to induce motion of magnetic nanoparticles, labeled inside a tissue mimicking phantom, and then Ultrasound is used to detect the induced motion of the labeled magnetic nanoparticles. However, the motion of these magnetic nanoparticles happens to provoke motion on surrounding regions where they are labeled. And we have a hypothesis that this motion of the surrounding regions is a mechanical reflection which is due to the conservation of mass within the phantom volume, and we want to understand what is happening and also verify that this is the case, which is why this project is undertaken.

The project aimed at building simulations besides experimentation in the lab. We have managed to do both the simulation and experimental work, and we hope that having both would help understand better the situation inside the phantom where the magnetic inserts are labeled.

2, Background Theory

2.1 Physics of ultrasound

Ultrasound waves are dependent on high frequency sounds, which cannot be sensed by human's ear. This high frequency sound travels through different media, like solids, liquids and gases, but not through vacuum. Depending on the material sound travels through, the speed varies. For instance, the speed of sound in water and in air is about 1482m/s, 343m/s respectively at room temperature [4]. Sound wave is a mechanical wave motion that requires a medium to propagate unlike light waves, which can even travel through vacuum. So, to propagate ultrasound a medium which is basically a fluid is needed to couple the transducer face, which to be discussed below, and the object of interest (skin). If in anyway air exists between the transducer face and the skin, the sound wave will not be transmitted

This mechanical disturbance wave propagates by longitudinal motion and within this wave compression and expansion occurs. The compression corresponds to high pressure and amplitude, whereas the expansion is a low pressure. When ultrasound is raised, mentioning the sound wave properties is inevitable and described as follows.

2.1.1 Wave propagation

Wave propagation is basically based on the time varying deformations or vibrations in materials [19]. It is the atoms, which vibrate, that all the materials are made of. So the propagation of a wave on a material is based on its atomic vibrations. Considering the sound wave, it focusses on particles that comprise atoms that move in harmony to produce mechanical wave. When atoms in a material are not moving they stay at their equilibrium position, which means that no external force is applied to displace these atoms. But when they are displaced up on the exertion of a force, they always experience internal restoring force which pulls them back to their equilibrium position. So it is this restoring force in accord

with inertia of the particles that create vibrational motion of the atoms and in turn on the material. Sound waves could propagate in solids in different ways but now it is important to consider longitudinal wave as it is most widely used in ultrasound, and transversal wave, even though it is not used quite often unless for special cases.

2.1.2 Modes of propagation

2.1.2.1 Longitudinal waves

This wave is characterized by the direction of oscillation, which is the particles vibration of the material are in the same direction as the direction of travel of the wave. Longitudinal wave travels in the form of compression and rarefaction. During propagation, a compression occurs when the vibrating particles come closer and in this case the distance between the particles becomes smaller than their normal distance. This leads to a temporary decrease in volume, which in turn increases the density of the particles in the region. Whereas, rarefaction occurs when particles move farther apart, and in this case the density of the particles decrease as the volume increases in the region [5]. Sound waves could be taken as an example. Here the particles move forward and backward along the direction of travel of the wave. The speed of sound waves in a solid is usually dependent on the elasticity property of the solid, like the young's modulus and density of the material. For sound waves through a thin bar, the speed is given by:

$$v = \sqrt{\frac{Y}{\rho}}, \text{ or generally, it is given by } v = \sqrt{\frac{C}{\rho}}$$

Here C is the elastic property of a material, like the bulk modulus or the Young's modulus, and has a unit Pa or N/m², v is the speed of sound, Y is the young's modulus and ρ is the density of the material. Here one can see that the stiffer the material is, the faster the speed becomes [6].

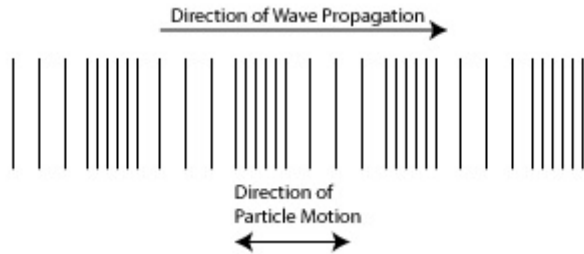


Figure 2.1: A longitudinal wave showing compression and rarefaction [7].

2.1.2.2 Transversal Waves

Unlike longitudinal waves, in a transverse wave the particles in a medium vibrate in a direction perpendicular to the direction of propagation. This means that, the particles are moving either up or down or from side to side as the wave goes forward [8]. A vibrating string could be taken as an example.

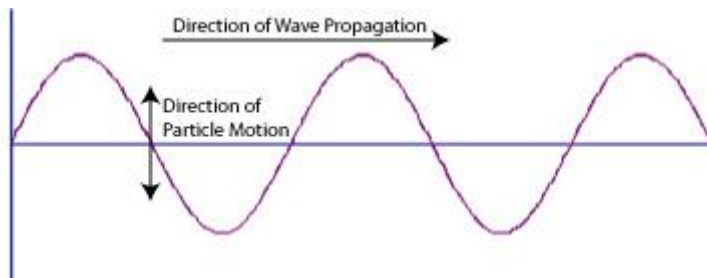


Figure 2.2: A transverse wave showing particles movement perpendicular to direction of propagation [7].

2.1.3 Wavelength, frequency and speed

A wavelength represents the distance between two successive high pressure pulses or low pressure pulses. Wavelength is designated by (λ).

This wavelength determines the penetration depth and resolution of ultrasound wave [20]. Frequency (f), is basically the most significant characteristics of sound, the rate at which the sound source and the material vibrate. It is the number of wavelength that pass per unit time and it is measured as cycles per second or hertz (Hz). This frequency is the specific feature of the crystal used in ultrasound transducer.

The propagation speed of a sound that travels through a medium is typically 1540 m/s in soft tissue and 3400 m/s in bone. The speed is determined solely by the medium characteristics, especially by the tissue density and stiffness. Generally, one can say that ultrasound travels faster in dense materials and slower in compressible materials. Frequency, wavelength and velocity of sound are related in the following way [21]

$$v = \lambda f \quad (2.1)$$

The wavelength is inversely proportional to the frequency. i.e. higher wavelength means lower frequency and vice versa.

2.1.4 Transducers

Transducers are devices that convert one form of energy to another, and focus the beam of pulses, so that it forms a specific size and shape at various depths within the body.

Ultrasound transducers convert electrical signals into sound signals and vice versa. Ultrasound waves are produced by a piezoelectric crystal, which is contained in the transducer element, a device which generates an electric potential in response to applied mechanical wave stress; this ability of the crystal is referred to as piezoelectricity. This crystal can also converts an electrical signal into ultrasound waves, pick up the reflected signal and convert back to electrical signal. This electrical signal will further be analyzed to make images [9]. The piezoelectric effect describes what happens when high voltage comes in contact with a transducer; it produces a mechanical shock wave. When this wave propagates to the

target, most gets attenuated and absorbed by the medium and these do not contribute to the image formation. But signals that hit the target will be partly reflected back to the transducer and converted into an electrical current and get amplified for further analysis and image formation.

2.2 Magnetic field

A magnetic field is a region around a magnet, in which a magnetic force may be exerted. Basically, a magnetic field is created by a moving charged particle. If one considers a long straight wire, and if current flows along this wire, then there will be a magnetic field created around this wire due to the motion of the charged particles through the wire. The relation between magnetic field and current is given by the Biot-Savart's formula as follows:

$$d\vec{B} = \frac{\mu_0}{4\pi} \left(\frac{Idl \times \hat{r}}{r^2} \right) \quad (2.2)$$

dl is the differential element of the wire, $\hat{r} = \vec{r}/r$ is the unit vector directed towards the point magnetic field from the differential element dl . B is the magnetic field, I is the current through the wire, and $\mu_0 = 4\pi * 10^{-7}$ T m/A is the permeability of free space, r is the distance to a point from the current carrying wire where the magnetic field is calculated [12]. This formula states that, the magnetic field at a point away from the wire decreases with the square of the distance. Once the magnetic field is calculated for the little element $d\vec{B}$, and integrating over the whole length of the wire will give you the total magnetic field at that point.

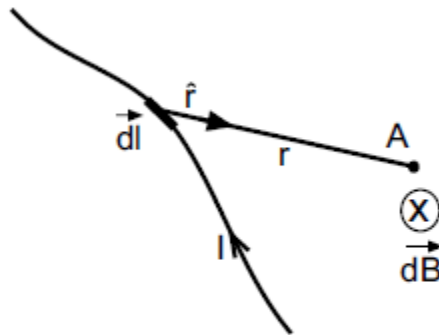


Figure 2.3: Illustration of the Biot-Savart Law [10]

Magnetic field is also created by a solenoid, which is a long current carrying wire having a large number of close turns of insulated copper wire. The magnetic field created this way is dependent on some parameters. According to Ampere's law; if we integrate the magnetic field along some closed path, then it has to equal to the product of the magnetic permeability of free space and the current with in the boundary of the path.

$$\text{i.e. } \oint B \cdot dl = \mu_0 I \quad (2.3)$$

Using the above equation (2.3) one can prove that, the magnetic fields created inside a solenoid is very much stronger due to the individual coil contribution, which adds up together to form a strong field and is given by :

$$B = \mu_0 \left(\frac{N}{L} \right) \quad (2.4)$$

Where N , is the number of turns; L is length of the solenoid, I is the applied current

As the above equation (2.4) shows, the magnetic field inside the solenoid is proportional to both the number of turns per unit length and the applied current. The applied current could also be time dependent and varies according to the formula below, which in turn changes the magnetic field sinusoidally.

$$\text{i.e. } i_0 = i_0 \sin wt \Rightarrow B = \mu_0 \left(\frac{N}{L} \right) i_0 \sin wt \quad (2.5)$$

The field outside the solenoid is very weak and its magnitude could be calculated by using the Biot-savart's law given in equation (2.2). A solenoid could have air or iron as a core material. When using air core solenoid smaller magnetic field is produced, but much higher magnetic field can be created by using an iron core or electromagnet, which is a soft iron core placed inside a solenoid and it becomes magnetized or acts as a magnet only when current flows through the coil, and gets demagnetized when current stops flowing[11]. The best thing about electromagnet on top of producing very strong magnetic field is; the magnetic field itself can be controlled by varying the number of turns of the coil and also by changing the applied current passing through the coil, as it is dependent on both. And this project uses a conical shaped electromagnet to guide the magnetic field, so that we can achieve a more concentrated field at the tip of the core.

2.3 Magnetic susceptibility

Magnetic susceptibility is the degree to which a material gets magnetized when it is exposed to an applied magnetic field. Materials, including human tissue can be characterized by their magnetic volume susceptibility, which is designated by the symbol χ . And it is defined by the relation:

$$M = \chi H \quad (2.6)$$

Where M , is the magnetization and H is the magnetic field strength. On the basis of the susceptibility values, materials could be classified in to three as diamagnetic, paramagnetic and ferromagnetic.

Diamagnetic is the property of a material which causes a magnetic field in opposition to an externally applied magnetic field. Diamagnetic materials have a negative susceptibility, that goes from -1 to 0 or $-1 < \chi < 0$. Biological tissue could be taken as an example. Its magnetic susceptibility value is

very small and is about $\pm 20\%$ of the susceptibility value of water, which is -9.05×10^{-6} [13].

These materials repelled from regions where there is high magnetic field. Those materials which have a positive susceptibility are referred to as paramagnetic, and unlike diamagnetic materials, they are slightly attracted to regions of strong magnetic field but they do not retain their magnetic behavior after the external magnetic field is removed.

There is another class of material in which its susceptibility value is positive and greater than the value that paramagnetic has and it is referred to as ferromagnetic or simply magnetic. These materials exhibit strong attraction to an applied magnetic field and they seem to keep or retain their magnetic properties after the applied magnetic field has removed. These materials do not show their magnetic properties unless they are exposed to external magnetic field and they are also called soft magnetic materials.

Compared to ferromagnetism and paramagnetism, diamagnetism is considered to have a very weak effect and it can be used to levitate objects despite its weak effect. Among some materials that exhibit diamagnetism, copper could be taken as an example, and unlike other magnetic materials copper could slightly be repelled by a magnet. Considering those materials of the like ferromagnetic and magnetic, which has a susceptibility in the order of one or greater, are very much responsive to applied magnetic field and could create danger if they are present in imaging modalities like MRI scanners [13].

2.4 Magnetic nanoparticles

Magnetic nanoparticles have been researched for years, are currently serving as a contrast agent for different biomedical applications, such as magnetic resonance imaging (MRI) [30], ultrasound imaging [2, 28] and photo acoustic imaging [31]. Such particles are easy to easily track and

manipulate using an external magnetic field produced by an electromagnet. Moreover, these particles recently have been used for different purposes such as drug delivery, cell separation, hyperthermia treatments of malignant tumors and also as contrast enhancement for MRI. Considering hyperthermia, once the magnetic particles are labeled in the tissue of interest, then time varying magnetic field is used to warm up the tissue and cause destruction of the malignant cells [22].

Nanoparticles have been chosen as contrast agents for different reasons. If to describe some of the main reasons, they are controllably small sized, which helps them attach to a tissue cell of interest, ranging up to tens of nanometers. It is noted that these particles perform best and act as a single magnetic domain, a region in a magnetic object where the magnetic moments act in the same direction, when their size is below some critical value, which is usually about 10-20nm, though this size is dependent on the material used. The critical value (radius) is given by $r_c \approx 9 \frac{(Ak_u)^{1/2}}{\mu_0 M_s^2}$, where A is the exchange constant, k_u is the uniaxial anisotropy constant, μ_0 is the permeability constant, and M_s is the saturation magnetization [14].

Most of the magnetic nanoparticles used as contrast agents in many biomedical applications are of super paramagnetic iron oxide (Fe_2O_3 or Fe_3O_4) and this is because of their capability not to retain magnetic behavior after the removal of the magnetic field.

The iron properties of magnetic nanoparticles could be improved by putting materials for instance nickel, cobalt and irons a core material, but these materials have their own limitation when it comes to biomedical applications, especially to put them into human body. That is, these materials could be toxic and also be very susceptible to oxidation. So instead it is other core materials such as iron oxide (Fe_3O_4) and Maghemite ($\gamma\text{-Fe}_2\text{O}_3$), which are not toxic and have high oxidative stability in use for medical applications. However, in general the core materials used in magnetic nanoparticles is dependent on the application [23].

2.5 Magnetic force and energy

A magnetic object basically experiences a magnetic force, which tends to move it, when it is placed in a magnetic field and also a torque which makes it rotate with respect to the field. These movements and alignments with respect to the field are not only dependent on the nature/susceptibility of the material but also on the strength of the field. Let's consider an object which has a magnetic characteristic and loaded in some tissue; when this object is exposed to an external magnetic field, having a magnitude of B , it acquires a magnetic energy U provided that the object has a magnetic moment m . This is a vector quantity that describes and measures the ability of the magnetic nanoparticles to align themselves with the magnetic field lines, it is proportional to the applied field and gets an induced moment m . The magnetic energy would then be given by

$$U = \frac{1}{2} \vec{m} \cdot \vec{B} \quad (2.7)$$

Where \vec{m} , is the magnetic moment and, B is the magnetic flux density.

For uniform magnetization over the volume of the object and assuming that the object has some volume V , susceptibility χ and its magnetization M is given by equation (2.6). As shown in equation (2.7), the magnetic energy is dependent on both the strength of the magnetic moment and the magnetic field and also on the angle between the magnetic moment and the field as both are vectors. The force exerted by the magnetic field increases the magnetic energy and this effect of the force attracts the paramagnetic materials towards the strong magnetic field and pushes the diamagnetic tissue towards the weak magnetic field region. The magnetic field energy equation will come down to:

$$U = -\frac{\chi V}{2\mu_0} |\vec{B}|^2 \text{ after having expressed the moment as } \vec{m} = \frac{\chi V}{2\mu_0} \vec{B}. \text{ And from}$$

this, one could express the force exerted on the object as $F = -\nabla U$, which

is the negative gradient of the magnetic energy giving $F = -\nabla \left(-\frac{xV}{2\mu_0} |\vec{B}|^2 \right)$. This equation is not simplified yet; however, it shows the dependence of the force on the gradient of the magnitude square of the magnetic field and some magnetic properties of the object [15, 24].

2.6 Magnetic Force acting on magnetic nanoparticles

To have a good understanding of how magnetic field is used to trap magnetic nanoparticles, it is necessary to discuss a bit of some theoretical background on magnetic field gradient and related vector fields. Magnetic field gradient is basically determined by the rate of change of magnetic field over distance, and a high gradient is experienced by magnetic particles when they are close to the field gradient, and when placed further away from the gradient, low field will be experienced. For a force to act at a distance on a particle or in order to generate force on a magnetic particle, having a magnetic field gradient is absolute necessity. Having a field which is homogeneous or uniform everywhere, wouldn't create a force on the particles as it has zero gradient.

Considering a magnetic particle that has a magnetic dipole moment m in a magnetic field B in the z -direction, then the magnetic force acting on this particle will be given by:

$$F_m = (\vec{m} \cdot \nabla) \vec{B} \quad (2.8)$$

So here it is assumed that the magnetic moment (m) is directed along the positive z -axis. That is $\vec{m} = (0, 0, m_z)$, which could then leads to

$\vec{m} \cdot \nabla = m_z \frac{\partial}{\partial z}$. So from here the magnetic force can again be expressed as $F_m = (m_z \cdot \nabla) \vec{B}$. In the case of a diamagnetic medium such as water or tissue, the total magnetic moment could be written as $m_z = V_m M_z$, where V_m is the volume of the particle and M_z is its volumetric magnetization, which

in turn can be written as $M_z = \chi H_z$, where χ is the susceptibility of the particle relative to the medium and is given by:

$$\chi = \chi_{\text{nanoparticle}} - \chi_{\text{medium}}$$

Having substituted $\vec{m} = \frac{\chi V}{2\mu_0} \vec{B}$ in equation (2.8), the force equation will

come down to [22]:

$$F_m = \frac{V_m}{\mu_0} \chi (\vec{B} \cdot \nabla) \vec{B} \quad (2.9)$$

As there are no time dependent electric fields in the medium the Maxwell's equation $\nabla \times \vec{B} = \frac{1}{c} \frac{\partial \vec{E}}{\partial t}$ reduces to $\nabla \times \vec{B} = 0$, then we can apply this to the vector dot product identity:

$$\begin{aligned} \nabla(\vec{B} \cdot \vec{B}) &= 2\vec{B} \times (\nabla \times \vec{B}) + 2(\vec{B} \cdot \nabla) \vec{B} \\ \Rightarrow \nabla(\vec{B} \cdot \vec{B}) &= 2(\vec{B} \cdot \nabla) \vec{B} \\ \Rightarrow \frac{1}{2} \nabla(\vec{B}_z \cdot \vec{B}_z) &= (\vec{B}_z \cdot \nabla) \vec{B}_z = \vec{B}_z \cdot \nabla \vec{B}_z = \vec{B}_z \left(\frac{\partial B_z}{\partial z} \right) \end{aligned}$$

The above force equation (2.9) could then be written as:

$$F_{mag} = \frac{V_m}{\mu_0} \chi B_z \left(\frac{\partial B_z}{\partial z} \right) \quad (2.10)$$

In the force equation (2.10), it can be seen that the magnetic force is dependent on the magnetic flux density and its gradient, and also some constants which are the magnetic properties of the material [22].

Considering the effect observed or the mechanical motion of both on the magnetic nanoparticles and the surrounding tissue mimicking phantom which is basically actuated by an externally applied magnetic field is described shortly in the following way.

The magnetic force acting on the magnetic nanoparticles, having a volume V and magnetization M , is induced from the externally applied magnetic flux density B having a gradient directed along the z -axis, is given in equation (2.10). In the same way as the force influences the magnetic nanoparticles (MNPs), the surrounding medium (e.g. tissue phantom) is also influenced by the magnetic force, which in this case is dependent on the volume magnetization of the medium. The magnetic forces acting on the MNPs and the surrounding are different, and so are their responses, as the gradient decreases away from the source. i.e. as the nanoparticles are magnetic, their response is paramagnetic and on the other side the response from the surrounding medium is very much lower, and be pushed towards the low magnetic field gradient. Moreover, the volume magnetization of the surrounding will have a sign opposite to that of the volume magnetization of the magnetic nanoparticles and this would create an out of phase movement between the MNPs and the surrounding. Besides here the viscous property of the surrounding shouldn't be forgotten. Generally, it is easy to say that the force acting on the surrounding medium balances the force experienced by the nanoparticles only when the number of magnetic particle density present in the medium is sufficient enough. The critical particle volume density is written in the following way:

$$\rho_{crit}(B) = N_p V_p = \frac{-M_m(B)}{M_p(B)} \quad (2.11)$$

where N_p is the number of MNPs, V_p is the volume, M_m and M_p are the magnetization of the surrounding medium and the magnetic nanoparticles respectively [26].

Labeling the medium with more magnetic nanoparticles, greater than the critical particle volume density, will allow the whole medium to move towards the high magnetic field gradient, and for a concentration less than the critical particle volume density will make the motion of the whole medium towards the low magnetic field gradient or the medium will have a diamagnetic response. So having a proper particle concentration would help to balance the two forces, and the MNPs to move towards the field while the surrounding goes away from the field gradient [26].

As mentioned above, when the magnetic nanoparticles are exposed to an external magnetic flux density, the randomly distributed nanoparticles start to respond and align their magnetic moment in the direction to the magnetic field. This reaction to the magnetic field is basically dependent on the nature of the material, in which these nanoparticles are labeled, like the viscoelastic property. The degree of the material being viscous affects the movement of the particle in reaction to the magnetic field.

The magnetic flux density acting on magnetic nanoparticles could be given by the following formula:

$$B = \mu_0(H + M) \quad (2.12)$$

where M is the magnetization of the magnetic nanoparticles, which is the magnetic moment per unit volume ($M = m/V$). Magnetization can also be expressed as the product of the magnetic susceptibility and the field strength as in equation (2.6).

For a diamagnetic medium, the magnetization M_m shows a linear dependence with the magnetic field strength H and this happens for field strength less than several tesla. However, in a magnetic medium the magnetization of the magnetic nanoparticle M_p show a nonlinear relationship with the magnetic field strength after saturation, which is usually above 2T but for very low field strength, the M_p is linear. So, this nonlinear dependence after saturation between the magnetization of MNPs and the field strength is best described by the Langevin function [15].

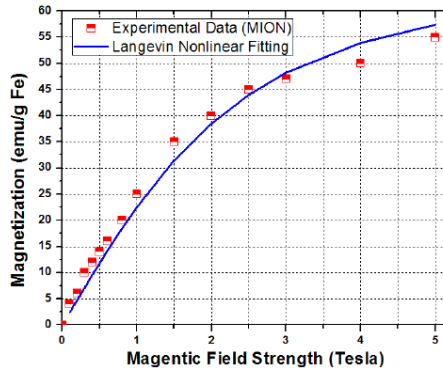


Figure 2.4: Magnetization as a function of magnetic field strength for magnetic iron oxide nanoparticle (MION) [15].

2.7 Motion of Magnetic nanoparticles

Upon the exposure of magnetic nanoparticles to an external magnetic field, the particles experience forces. If to consider only the z-directional or vertical component forces, as ultrasound measures only vertical component, it is seen that there are three forces acting on the particles. These forces are; the magnetic force which basically drives the magnetic nanoparticles towards the highest gradient field, the elastic restoring force and the viscous drag force. The elastic restoring force is a force developed inside the particle when it is strained or deformed and makes the particle to attain its original shape or restore it back to the original position. The viscous drag force is like a frictional force that opposes the direction of motion and in this case it is the tissue mimicking phantom where the particles are embedded in. Both the viscous drag force and the elastic restoring force act in opposite direction from the magnetic force. All the forces are given in the following way:

$$\sum F_z = m \frac{\partial^2 z(t)}{\partial t^2} = F_m - kz(t) - r \frac{\partial z}{\partial t} \quad (2.13)$$

Here F_m is the magnetic force acting on the nanoparticles and it is directed towards the field gradient, $kz(t)$ is the elastic restoring force and $r \frac{\partial z}{\partial t}$ is the viscous drag force [15,18].

2.8 Tissue magnetic field interaction

As defined above, magnetic field is a field produced basically by an electromagnet or moving charged particles. This field could be either static or time dependent.

Magnetic fields interact with human body in different ways, but before mentioning them let us see to what extent humans are exposed to magnetic field. We all are exposed to magnetic field in our daily activity; to consider some, from home appliances where electricity exists and also from the magnetic field of the earth, which is produced due to the motion of the molten iron inside the core. This field is static but varies in different places of the earth. Its average magnitude would reach to 50 microtesla, which is very small to be noticed by humans but it can be noticed by some animals and they use it for their orientation. Though nowadays, we are being exposed to a very high magnetic field when using the magnetic resonance imaging (MRI) as a therapeutic technique. This technique was introduced in the beginning of 1980s. Since then it has been used to make pictures of body structures and organs thereby getting the necessary information out of it. The MRI technique uses a magnetic field strength of up to 3T, which is about 60,000 as high as the earth's magnetic field, for human imaging. However, in recent time field strengths above 3T is being utilized for research purposes [13, 24].

The generation of electric fields and currents in the vicinity of the blood vessels, which is produced due to static magnetic field force acting on moving charges in the blood, could lead to the hampering of blood flow and this basically varies depending on the alignment of the field with the blood flow and also the strength of the field. i.e. when the magnetic field is

perpendicular to the blood flow the effect could be large but when it is parallel to the blood flow smaller effect would be expected. It is found out that the reduction of blood flow in the aorta for a perpendicular field could reach to 1%, 5% and 10% for a 5T, 10T and 15T respectively. This could be taken as one way of body tissue interaction with magnetic field. The other could be when metallic objects are implanted inside a body as a pace maker or for some other purposes, which probably would lead to a serious damage to body tissue when exposed to a static magnetic field. The one thing that should be mentioned is the body motion in a magnetic field, which creates an electric field and currents in the body. For a static electric field \mathbf{E} in a medium having an electrical conductivity σ , the current density is given by:

$$\mathbf{J} = \sigma \mathbf{E} \quad (2.14)$$

But when the body tissue is moving with some relative velocity in the static field, the current density would add a motion induced electric field term $\mathbf{V} \times \mathbf{B}$ and would be written as:

$$\mathbf{J} = \sigma (\mathbf{E} + \mathbf{V} \times \mathbf{B}) \quad (2.15)$$

So, having body motion in or out of a magnet could create a risk to the body tissue [13, 27].

2.9 Tissue ultrasound interaction

The interaction of ultrasound with tissue can be described by the following terms; attenuation, reflection and refraction. When sound travels through a medium it gets attenuated, and this attenuation basically describes how sound is absorbed, dissipated and the signal becomes weaker as ultrasound travels through the tissue. Sound having higher frequency has more attenuation and less penetration.

Reflection describes how ultrasound waves reflected from interfaces like tissue boundaries or generally when any sound wave travelling from one

medium on to another, some of the waves signal gets reflected at the boundaries of the first medium and this is because of the difference in acoustic impedance between the interfaces. Actually, those reflected signals from the second interface are converted back to sound waves and form images. The amplitude of the reflected and transmitted signals basically dependent on the acoustic impedance (Z) difference between the materials. If the material is soft tissue/ air, then most of the ultrasound signals would be reflected at the first material and less would be transmitted into the second material to produce echoes at the deeper regions that accounts for the ultrasound signal. So is true for soft tissue to bone boundary. This is because of the acoustic impedance mismatching, which is defined as the product of the density of the medium and the propagation speed of ultrasound through the medium and is given by:

$$Z = \rho v \quad (2.16)$$

That is, if the acoustic impedance difference between the two materials is large, then most of the signal will be reflected and less transmitted but if the acoustic impedance mismatch is small, a very small percentage of the signal will be reflected at the first material and more will be transmitted. This would explain why ultrasound is not used as an imaging technique for bone, digestive tract and lungs.

Having known the acoustic impedances of two media, one can calculate the fraction of the incident wave intensity or the reflection coefficient between the materials by using the following formula:

$$R = \left(\frac{z_2 - z_1}{z_2 + z_1} \right)^2 \quad \text{where } R \text{ is the reflection coefficient, } z_1 \text{ and } z_2 \text{ are the}$$

acoustic impedances of the respective media [16].

The following table shows the different acoustic impedances of various tissues:

Tissue	Acoustic Impedance (Rayl)
Air	0.0004
Fat	1.38
Water	1.48
Blood	1.61
Kidney	1.62
Soft tissue(Average)	1.63
Liver	1.65
Muscle	1.7
Bone	7.8

Table 1: Different acoustic impedances of various tissues [18]

Refraction describes the bending of the signal as it travels through two different media. What happens when ultrasound traverses through two materials is that some of the signals get reflected at the boundaries and some transmitted. So, it is this transmitted signal which undergoes bending and creates refraction. This refraction effect is usually responsible for ghosting of the image.

2.10 Contrast agents used in ultrasound imaging

Contrast agents are materials used in different imaging techniques, to improve or enhance the imaging quality of deeper structures within the body, mostly blood flow. Some decades ago nobody had a clue about ultrasound contrast agents and their discovery was accidental; it was an intravenous injection of saline solution that led to their being existence and

usage in today's ultrasound imaging. The micro bubble contrast agents, which are being used in ultrasound imaging, contained in the saline scattered the ultrasound signal in a more efficient way. This is because of the acoustic impedance mismatch between the micro bubbles and tissue cell. Micro bubbles contrast agents range in size from $1\text{-}7 \mu\text{m}$ [17], which basically is of size in the order of red blood cells. The micro bubbles being small sized allow them to reach the smallest capillaries. Contrast agents are injected through the blood stream to get better ultrasound reflection as blood is not a very good scatterer of ultrasound signal. As a result one would be able to see a good contrast on the image.

Commercially available micro bubbles could come in basically three different forms: micro bubbles filled with gas, liquid and solid. Gas filled micro bubbles scatter ultrasound signals much better than liquid and solid filled micro bubbles of comparable size. This is because of the acoustic impedance mismatch between the gas filled micro bubbles and the surrounding tissue where it is embedded. Also the compressibility of the gas makes the ultrasound signal scatter strongly. Mostly the gas filled micro bubbles are encapsulated with biocompatible materials like fat or protein; this is because the micro bubbles without shells tend to dissolve fast when they go through blood stream. So the encapsulation of the micro bubbles with fat or protein based agents help them to pass through blood and reach organ of interest. Properties, like the life time of the micro bubbles and their response to the ultrasound signal are dependent on the shell materials (fats and proteins) that enclose the micro bubbles [16].

Nowadays, micro bubbles are the most commonly used ultrasound contrast agents. When they are exposed to the ultrasound signal, the micro bubbles undergo oscillation. That is, they tend to contract and expand during compression and rarefaction of the signal respectively and also to vibrate at their resonance frequency, which is the frequency at which the micro bubbles oscillate easily. The effectiveness of the micro bubbles as ultrasound contrast agent is due to the coincidence that for micro bubbles having a size less than $7 \mu\text{m}$ corresponds to the frequencies used in diagnostic ultrasound imaging which is basically in between [2-10] MHz [17].

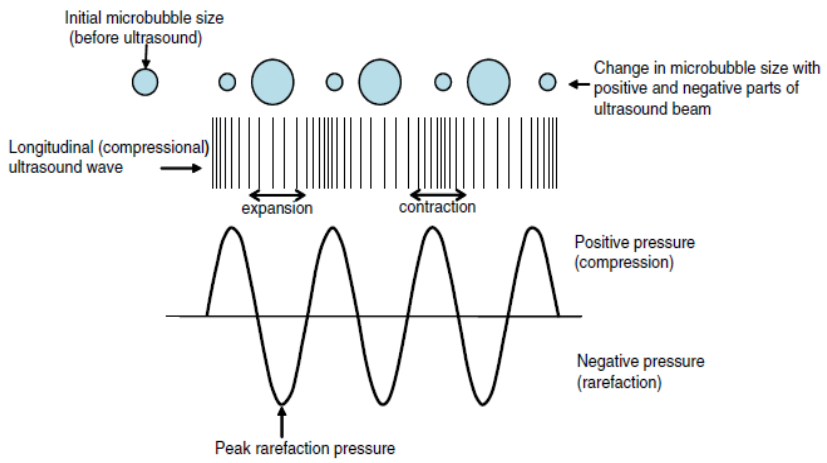


Figure 2.5: Contraction and expansion of micro bubbles in response to ultrasound signal [16].

3, Materials and Methods

3.1 Experimentation

3.1.1 The nanoparticles

The nanoparticles are synthesized by Genovis AB, Lund, Sweden. These nanoparticles were made of a solid iron oxide core (Fe_3O_4). A mixture of FeO(OH) fine powder, oleic acid and 1-octadecene was used to make the iron oxide core. This iron core is coated with polyethylene glycol (PEG, molecular weight 2000-4000g/mol) to stabilize the suspension. The magnetic saturation of the particle was approximately 80emu/g Fe_3O_4 and its diameter including the coating is measured to be 18 ± 2 nm [28].

3.1.2 Preparation of tissue mimicking Phantoms

The phantom was basically made in order to fulfill the basic characteristics of tissue, which are the optical scattering and elasticity. So, the phantom preparation started by having the aim that it should contain 5% by weight of the polymer polyvinyl alcohol (PVA) (average Mw 85,000-124,000, 98-99% hydrolyzed, sigma- Aldrich, USA). The preparation began by dissolving the crystallized PVA in MilliQ water in an autoclavable glass bottle sealed with a polypropylene cap, and then after the mixture was put, in (Nüve, Ankara, Turkey) FN300 oven, for about two hours at a temperature of 95 degree Celsius[28]. Once made sure that the crystallized PVA was dissolved in the MilliQ water, we took it out and added 30mg/ml solution of graphite (Graphite, Merck KGaA, Darmstadt, Germany) to act as a scattering medium. A magnetic stirrer was used to mix the solution well. The mix was then poured in to a phantom mold, which is a container made of Plexiglas. Three Plexiglas cylinders were attached on the side so that they can create holes for the three different concentrations. We have made five different concentrations: 0.1, 0.2, 0.3, 0.4, and 0.5mg iron oxide/ml of nanoparticle PVA inserts by using five

Eppendorf tubes. Once the five different concentrations were made and placed inside the Eppendorf tubes, the PVA solutions were added to it. Finally these mixtures were drawn to five syringes, which have the same internal diameter of 5mm as the holes created in the phantom. Before inserting these concentrations, three at a time as shown below on fig.3.1, the mixture had to go through two freeze/thaw cycles, to crosslink the mixtures.



Figure 3.1: Different set up of the inserts in the lab

3.1.3 Experimental set up

The MMUS imaging system used in this investigation is depicted in (Fig.3.2). This measurement was performed with a high-frequency ultrasound scanner, visual Sonics Vevo 2100 (Visual Sonics Inc., Toronto, ON, Canada). The magnetic field was generated by a solenoid (Ledex 6EC, Saia-Burgess Inc., USA) wrapped around a conical shaped iron core that focuses the field. A function generator (HP 33120, Agilent technologies, Santa Clara, CA, USA), which is connected to a power amplifier (in-house designed, 3db bandwidth 6-20000Hz) is used to adjust the electric current signal and in turn the strength and frequency of the applied magnetic field can be controlled. The signal to the solenoid was monitored with an oscilloscope (Tektronix TDS 360, Tektronix Inc., Beaverton, OR, USA) and the amplitude of the voltage was adjusted to be constant over the frequency range used [28]. Experiments were performed for different sinusoidal voltage having magnitudes 10, 20 and 30V with frequencies 4, 8, 12, and 16Hz.

The rectangular phantom was placed on top of the conical shaped iron core, and the gap separating them is about 1.5mm. That is, the phantom and the iron core are not actually in contact. The transducer, MS250 (13-14 MHz bandwidth, having central frequency 21MHz), was positioned just above the ultrasound gel applied on the surface of the phantom. The gel serves as a coupling medium allowing ultrasonic energy to travel freely between the phantom and the transducer head. If the gel was not used, it would be very much harder to pass ultrasound as ultrasound is highly absorbed by air, and also because of the acoustic impedance difference between the air and the medium.

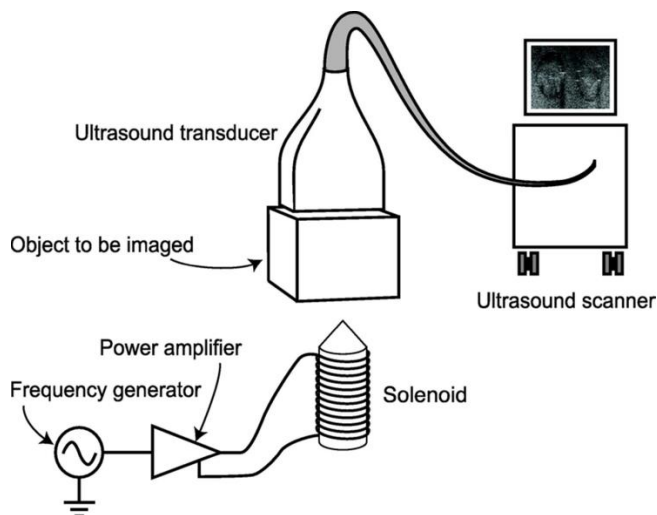


Figure 3.2: Schematic diagram of the MMUS imaging system experimental set up [28, 29]

3.2 Simulations

Before we start out describing the simulation procedure, it is important that we describe what it is like in the real experiment. The generation of the

magnetic field needs a generator, which produces current, a magnetic core, and a coil, wrapped around the core. A current passing through a wrapped coil on an iron core creates a magnetic field and since the core is conically shaped, the magnetic field be focused at the tip of the core. The current used to drive the electromagnet has a sinusoidal form given in the equation (2.5) above. So basically, this explains the first part of the simulation in the experiment. The second part uses this magnetic field force to manipulate the inserts placed inside a tissue mimicking phantom as depicted on fig 3.3 below.

3.2.1 Description of Comsol Program and its use in this project

Just to put it in simple words, Comsol is a program that allow scientists, engineers or generally us to simulate the effects observed in physical phenomena. So to do this, there is a need of multiphysics which is the multiple scientific models that can tackle problems in many fields of science and engineering. It is worth to mention some of them: electromagnetism, acoustics, magnetic field, structural mechanics, fluid dynamics and heat transfer. So this multiphysics program not only helps people to simulate the real world reflections but also helps us to simulate what we need in a much easier and faster way, and I would say that computer simulations and future technologies are vitally tied together.

The Comsol program was previously known by the name FEMLAB, which is a finite element method. This program comprises different programs in it, and all those programs were responsible to execute only one part of the modeling procedure. One program creates the geometry, another he meshing followed by other programs to do the solving and the post processing. This makes it a bit complicated to analyze or tackle a problem. So this is where Comsol program takes part and performs all the procedures; creating the geometry, meshing, solving and post processing in one program. This means all the items in one program which makes it very user friendly. So today, solving and visualizing physical phenomena has become possible by Comsol. These are some of the main reasons why we

have chosen this program to be used as a simulating program in parallel with the experimental lab measurement in this project.

This program has been used since the start of the project. Its main objective is to simulate the effect of a magnetic field on an insert/nanoparticle, with some magnetic characteristic placed inside some tissue mimicking phantom. Just to break it down a bit, the idea is to manage to move or oscillate the insert and thereby see the movement of the surrounding in response to the magnetic field that comes out at the tip of an iron core. A simulation would help us not only comparing the results obtained from the experimentation but also to understand what is going on inside, and to see the different effects observed when changing different parameters. All details and how it has been implemented in the project are described as follows.

3.2.2 Simulation procedures

3.2.2.1 Simulations of Magnetic field and Structural mechanics on 2D- axisymmetric

Basically the simulation is divided in to two parts; the first is the simulation of the magnetic field extending from the iron core tip, and the second part is the simulation of the structural mechanics depicting the movement of the nanoparticle laden tissue. The second part shows the nanoparticle loaded inside the phantom. This part of the simulation uses the magnetic field force as an input to manipulate the inserts and make them oscillate as explained in the material section.

3.2.2.1.1 Magnetic field simulation procedure and definitions

Both simulations have been done on a 2D-axisymmetric space dimension. The magnetic field simulation started by choosing the magnetic field interface from the add physics menu, after having set the space dimension. Then followed selecting presets, which help to choose the study type, for instance; the frequency domain, stationary, and time dependent. In this case, as we use a time dependent magnetic field, we set the preset to be time dependent. The next step is to add all the necessary parameters needed to make the simulation work on the global definitions section followed by making of the frame (geometry) as it is shown in Figure 3.3.

The rectangular cone shaped block, numbered as (1), represents the iron core, the next rectangular block (2) attached to the iron core shows the multi-turn coil wrapped around the iron core. The last rectangular region (3), comprising both the iron core and the multi turn coil represents the air. All the three domains have different material properties as they are made of different materials. The conical shaped geometry represents the iron core, which basically has a high permeability relative to the surrounding air and is also capable of multiplying the magnetic field a way better than air.

So once the geometry is done, the next step is meshing the whole geometry, after having labeled each domain to its respective material property. Having finished the meshing then the simulation is ready to run.

3.2.2.1.2 Structural mechanics simulation procedure and definitions

The structural mechanics simulation was done in the same way as the magnetic field. That is, first by choosing the physics solid mechanics, followed by choosing time dependent study interface and finally making the geometry needed to make the simulation work. The geometry is basically a rectangular block consisting of circles inside, which we assume it as inserts or magnetic nanoparticles. These magnetic nanoparticle inserts were labeled in a viscoelastic medium. The point here is to move the inserts, but there is not any external force that would make the inserts

displace. So, as we want to move it up and down, we added initial values, which have a displacement and a structural velocity field to make it displace. So here on the initial values field you can put by how much you want the inserts to be displaced and how fast to move. Figure 3.3 below shows the geometry used to make the structural mechanics work.

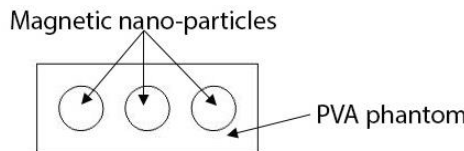


Figure 3.3: Structural mechanics geometry

The above procedures were implemented and once we were sure that both separate simulations worked, we started a new set up to simulate both physics simultaneously, i.e. coupling of the two physics. As in the same way explained above, it all started by choosing the two physics interface, the magnetic field and solid mechanics, followed by time- dependent study interface. Once these are set, the geometry for both the magnetic field and solid mechanics part is done and all put together in one rectangular region which we assume it as air. We started by labeling only one insert (magnetic nanoparticle) to make sure that the simulation works.

A few points on the materials used for the simulation should be mentioned; the tissue mimicking phantom and the inserts both have viscoelastic characteristics. Basically, both the phantom and the inserts have similar material properties, except for the insert containing some iron oxide nanoparticles. The materials share the following material properties: The young's modulus (describes the stiffness of elastic material), poison's ratio, electrical conductivity, density, relative permeability and permittivity. The inserts mentioned above act in the phantom as a body load, which is the calculated magnetic force per unit volume. This is what we used as a trick in the simulation to induce motion in the nanoparticle labeled tissue. The above material properties describe the structural mechanics part of the simulation. All these materials are enclosed in a rectangular region, which has the material characteristics of air. So, once all the necessary inputs are set the simulation is ready to run.

Figure 3.4 shows the geometry of the iron core and the coil wrapped around the iron core. The geometry is done on 2d axisymmetric space dimension. The magnetic field is coming out at the tip of the iron core where it gets focused. The coil, which in this geometry is the thin rectangular region attached to the conical shaped iron core, comprises many turns of copper wire. The system is driven by an alternating current (AC). When the current in the coil creates the magnetic field inside the iron core and thereby gets focused at the tip. Both the core and the coil are enveloped in another rectangular region assumed as air.

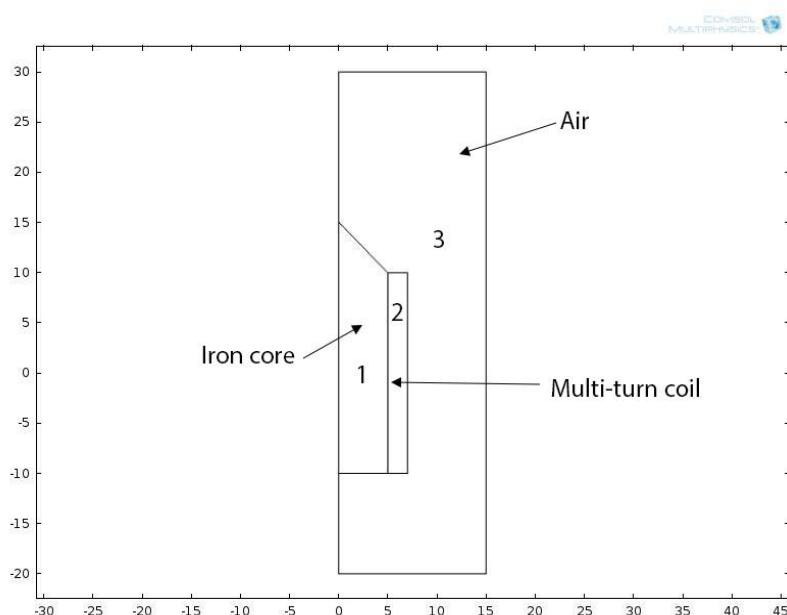


Figure 3.4: The picture shows magnetic field geometry on 2d-axisymmetric

3.2.2.2 Simulations of Magnetic field and Structural mechanics in 3D

Comsol FEM simulations program is used to model the set up for the magneto-motive ultrasound imaging. The model is designed with different dimensions for the different materials involved in the geometry. The first thing modeled was the conical iron core with 13.6 mm base radius and 34mm height from the base till the tip of the core. Following the making of the iron core, copper is used to enclose the iron core, which basically here has inner and outer radius 14 and 34.4 mm respectively, but this was done by revolving a rectangle, having a width of 20.4mm and 30.8mm height, around the conical shaped iron core. In the 3D simulation, besides the coupled magnetic field and structural mechanics, partial differential equations (PDEs) were added. The rationale for this is that the spatial field gradient cannot be calculated without the PDEs. To plot gradient of magnetic field in 3D, Comsol uses vector (curl) elements. The solution to these problems is the magnetic vector potential (\mathbf{A}). The magnetic flux (\mathbf{B}) involves the first derivative of \mathbf{A} and is given by the equation $\mathbf{B} = \nabla \times \mathbf{A}$.

However, the second derivative is not defined on vector elements and hence the spatial gradients of \mathbf{B} cannot be visualized directly in Comsol. So, this is where the PDEs are needed to calculate the gradient of the field along all the axes. The technique to visualize the spatial derivatives of \mathbf{B} is given below and the idea is to map each component of the magnetic flux density $\mathbf{B} = [B_x, B_y, B_z]$ to a separate variable say U, U_2, U_3 respectively.

The new variables would be defined on Lagrange elements. As both 1st and 2nd order derivatives are defined on Lagrange elements, one should be able to obtain spatial derivatives of each component of \mathbf{B} . This way the magnetic field gradient can be plotted.

Having finished making the geometry needed to make the magnetic field work, the structural mechanics geometry was continued; the first part was the making of the rectangular block with dimensions 10mm high, 10 mm wide and 25 mm in length. Finally the whole geometry was enclosed in one big rectangular block having dimensions 60, 80 and 80 mm in height, width and length, respectively.

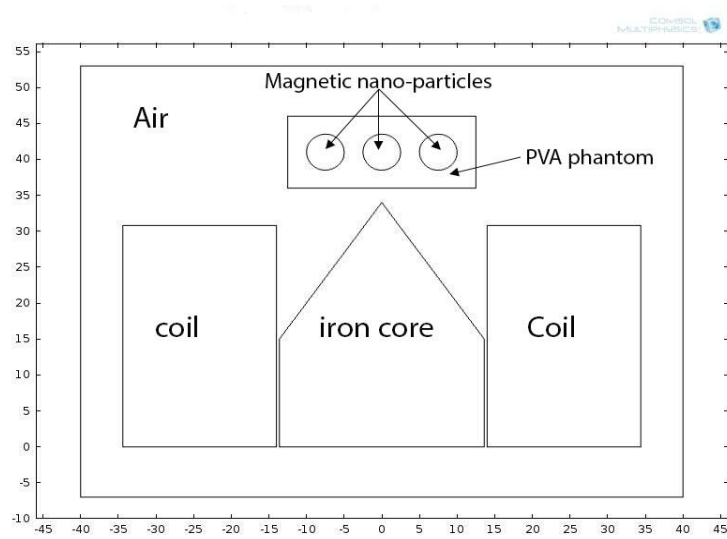


Figure 3.5: Slice picture of the 3D geometry

4, Results

4.1 Experimental results

The following results are obtained from the measurements performed on magnetic nanoparticles labeled inside a tissue mimicking phantom (PVA); the making of the phantom is explained in the material and method section. A focused magnetic field is used to provoke motion on the nanoparticles.

4.1.1 Experimental results from the high concentration set-up

Fig.4.1 shows the motion of the different concentrations of the nanoparticles, labeled in the PVA phantom, and also the surrounding area. Here it can be seen that the concentration of the iron (III) oxide (Fe_3O_4) in the middle insert straight above the tip of the iron core, is less than the concentrations of those on the side. After the magnetic field is turned on motion over the entire area is detected at a frequency range of (0-50Hz). The displacement of the whole area at these ranges of frequency is displayed in Fig.4.2.

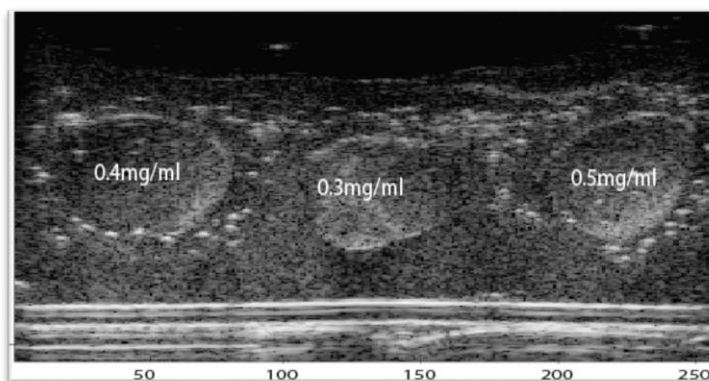


Figure 4.1: The B-mode image of the nanoparticle inserts labeled inside the PVA Phantom

All these displacements have taken with a frequency of 4Hz at 30V.

concentrations	disp@crosssection1 (micro meter)	disp@crosssection2 (micro meter)	disp@crosssection3 (micro meter)	Average disp (micro meter)
0.4	0.1687	0.2263	0.1387	0.1779
Between	0.3145	0.3571	0.2813	0.3176
0.3	0.4332	0.5565	0.4964	0.4954
Between	0.4568	0.3765	0.3227	0.3853
0.5	0.4614	0.3818	0.3023	0.3815

Table 2: Displacement of the inserts and the area in between for the high concentration

Fig.4.2 shows a color coded image of the motion of the entire phantom and the labeled inserts detected at all frequencies

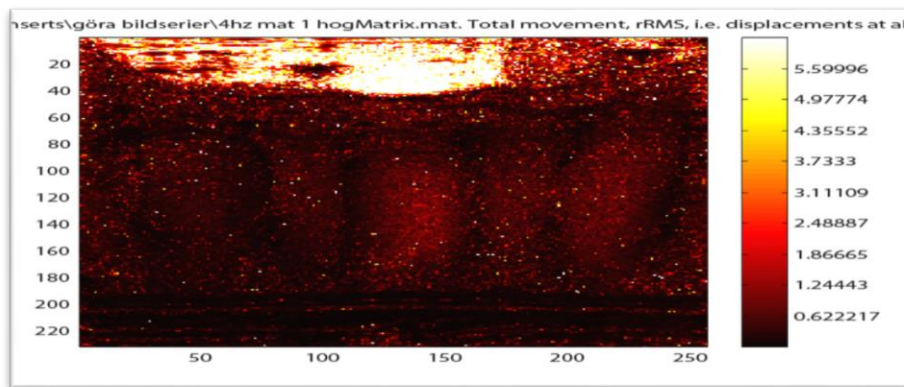


Figure 4.2: Motion of the whole area (the inserts and the surrounding) detected at all frequencies in micrometer (μm) scale.

Fig.4.3 shows the motion of the nanoparticles and the surrounding where the inserts are labeled. Here all the other frequencies are excluded, except for the 8Hz frequency. The iron laden inserts and the area in between are moving at a frequency 8Hz, which is twice the frequency of the magnetic field , and that is about 4[Hz].

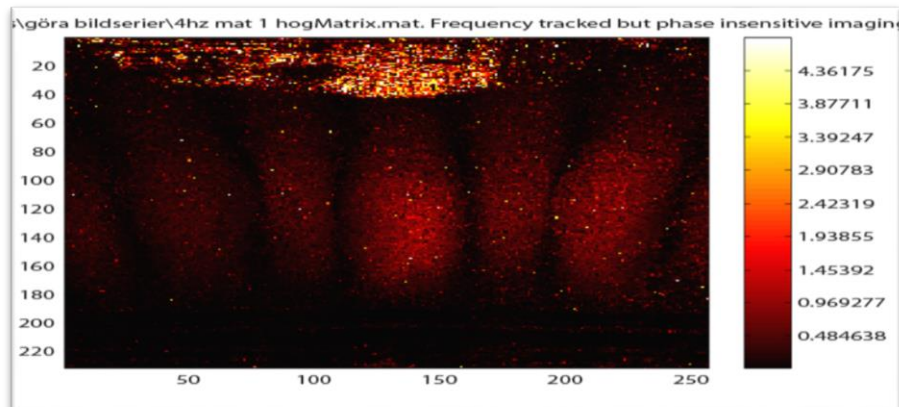


Figure 4.3: Motion displacement of the nanoparticles and the area in between in micrometer scale detected at a frequency of 8[Hz].

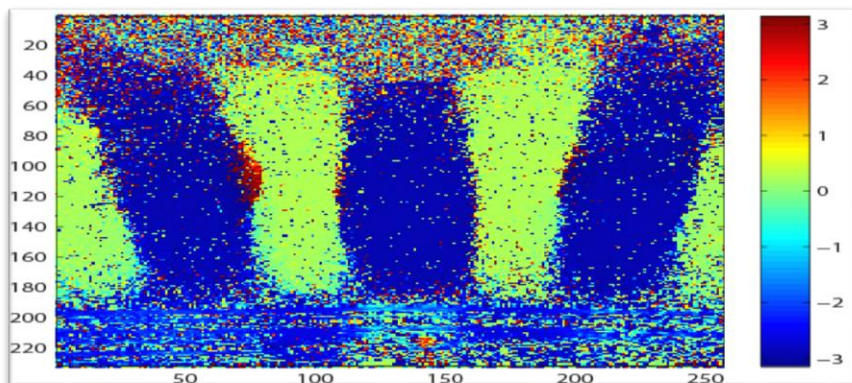


Figure 4.4: The phase of the inserts and the surrounding in radians.

The phase of the nanoparticle is color-coded with blue, whereas the region surrounding them is with yellow/green, here it shows that the magnetic inserts are moving with the same phase, and the surrounding region between the inserts and the wall moves with opposite phase from the inserts.

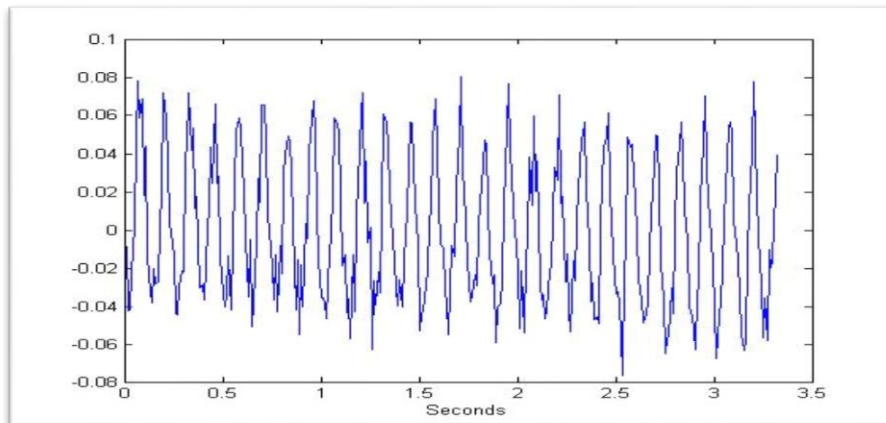


Figure 4.5: The sinusoidal motion of the iron-laden inserts

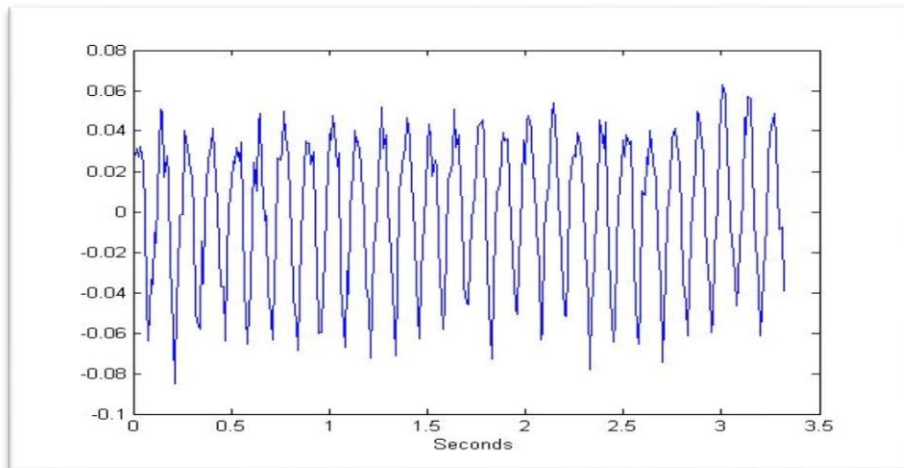


Figure 4.6: Sinusoidal motion of the area in between the iron-laden inserts

From fig.4.5 and fig.4.6, it can be seen that the motion in the inserts and the surrounding region are π radian out of phase.

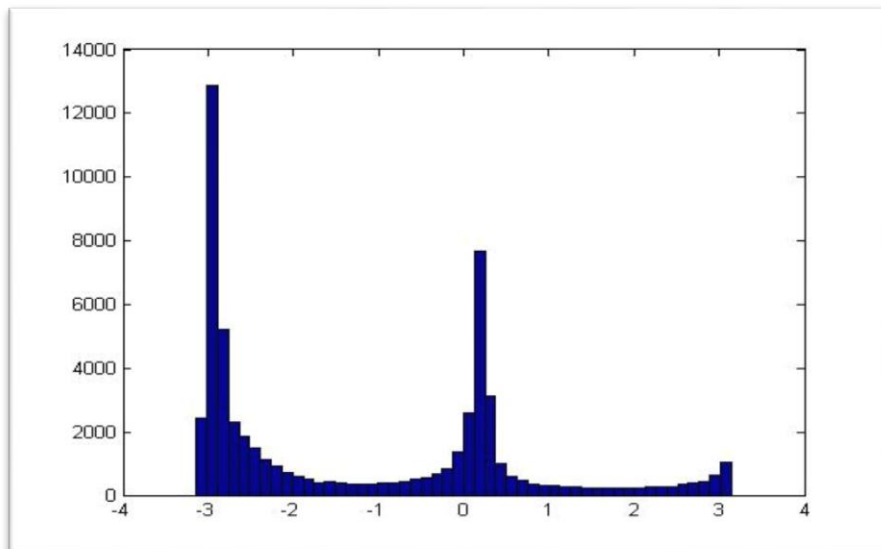


Figure 4.7: Histogram displaying different phase of the inserts and the region in between.

The vertical displacement of the inserts at a frequency of 8[Hz]

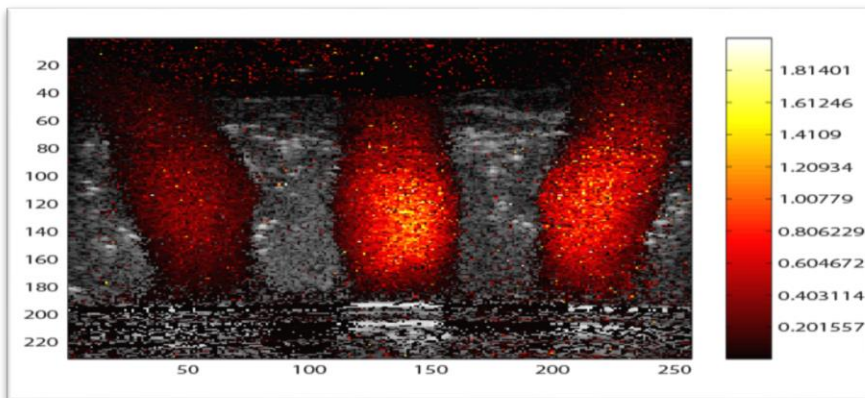


Figure 4.8: the displacement of the inserts in micrometer scale at a frequency of 8[Hz] displaying only the phase of the inserts

4.1.2 Experimental results from the low concentration set up

The picture presented in fig.4.1 is the same as in the fig. 4.9 below, the only thing different here is that the concentration of inserts labeled on the other side of the middle insert, 0.3mg/ml of Iron (III) oxide (Fe_3O_4), is less than those labeled in fig.4.1

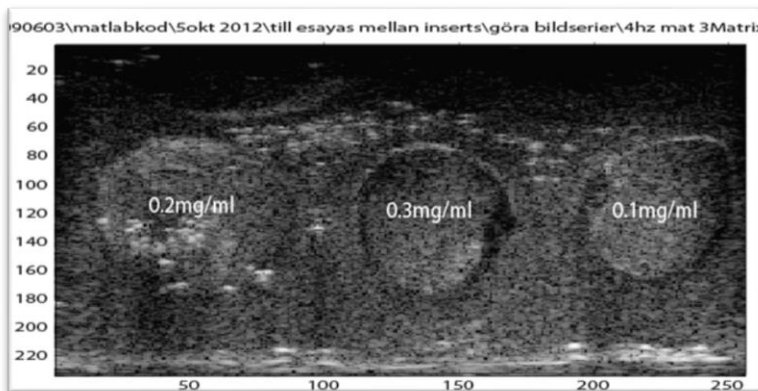


Figure 4.9: B-mode image of the low concentration set up

concentratio ns	disp@crossecti on1 (micro meter)	disp@crosecti on2 (micro meter)	disp@crosecti on3 (micro meter)	Avera ge disp (micro meter)
0.2	0.0409	0.0172	0.0537	0.0373
between	0.2415	0.2214	0.1872	0.2167
0.3	0.6972	0.6020	0.6841	0.6611
between	0.4135	0.2673	0.3393	0.3400
0.1	0.0139	0.0043	0.0164	0.0115

Table 3: displacement of the inserts and the area in between for the low concentration taken from three different cross-sections.

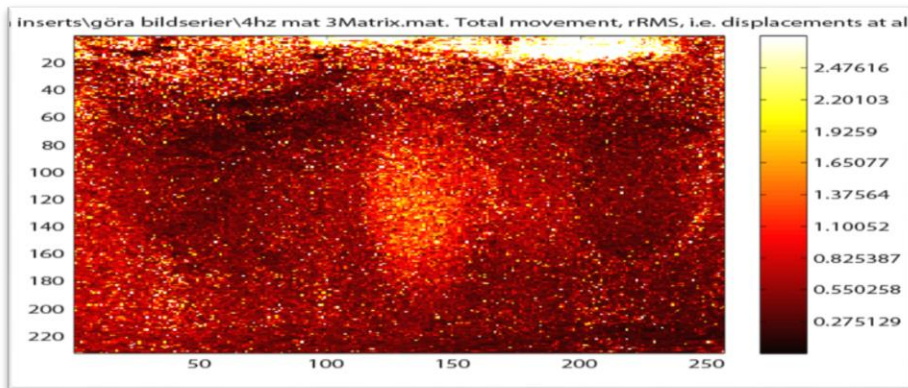


Figure 4.10: Vertical displacement of the inserts and the surrounding in micrometer scale at all frequencies

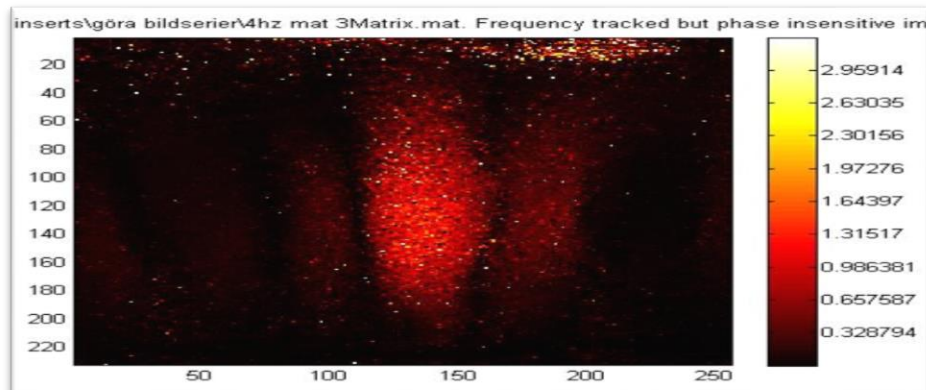


Figure 4.11: Vertical displacement of the inserts in micrometer scale at a frequency of 8[Hz]

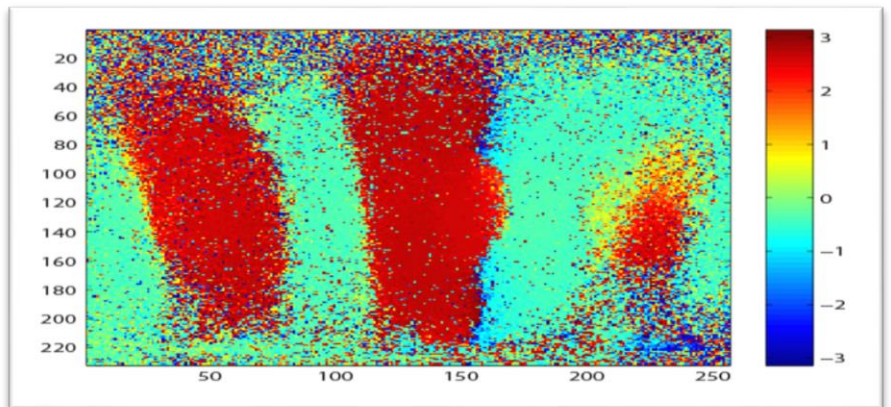


Figure 4.12: relative phase displacement of the inserts and the area in between measured in radians

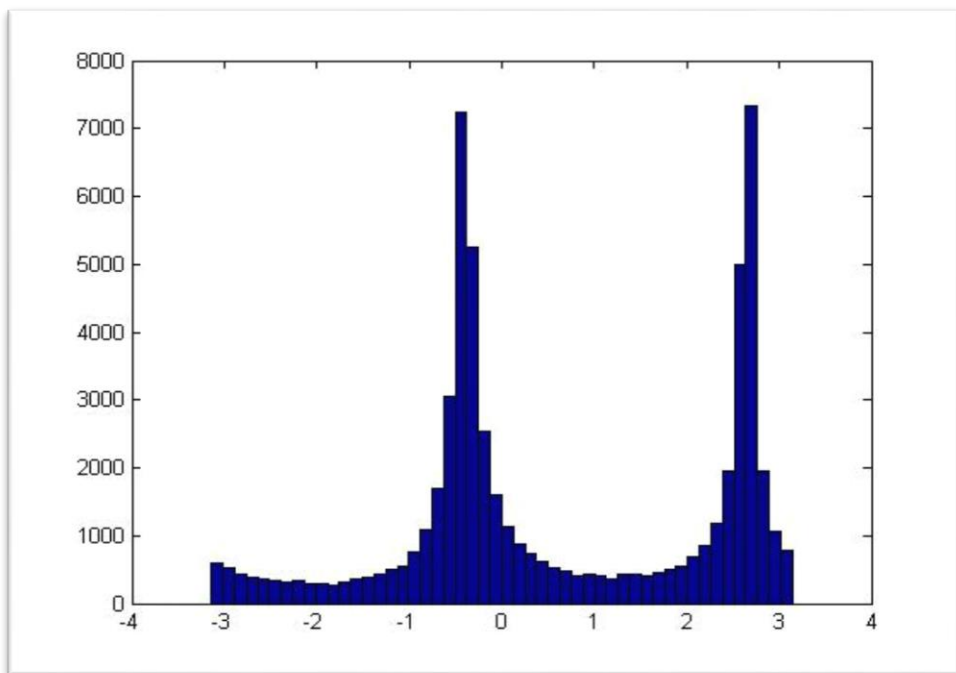


Figure 4.13: Histogram showing the opposite phase of the insert and the area in between

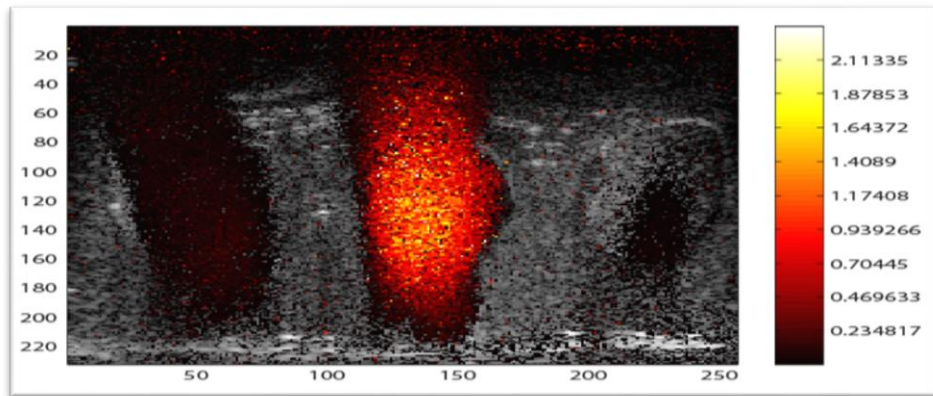


Figure 4.14: displacement of the inserts showing only the phase of the inserts excluding the area in between.

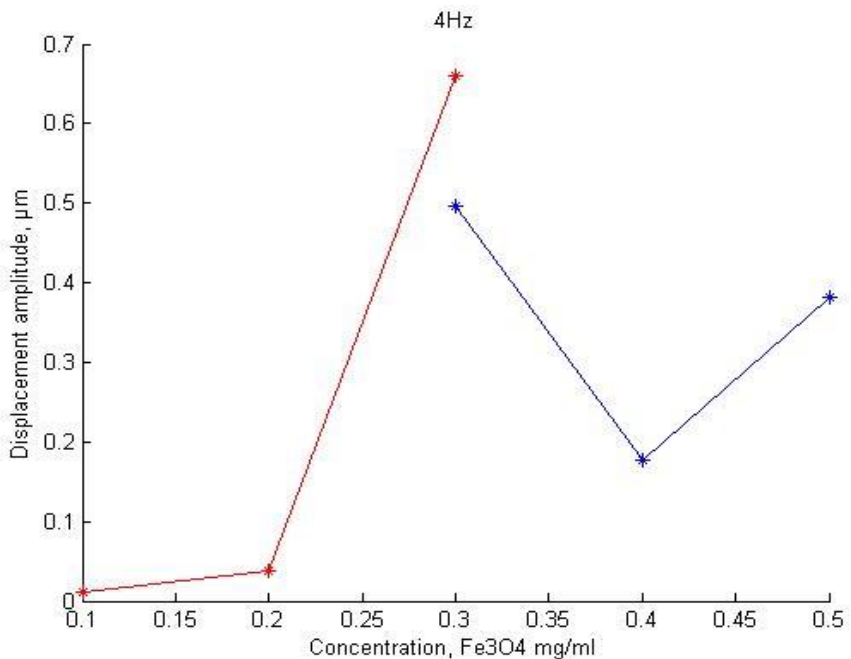


Figure 4.15: Displacement for the different concentration taken at a frequency of 4Hz

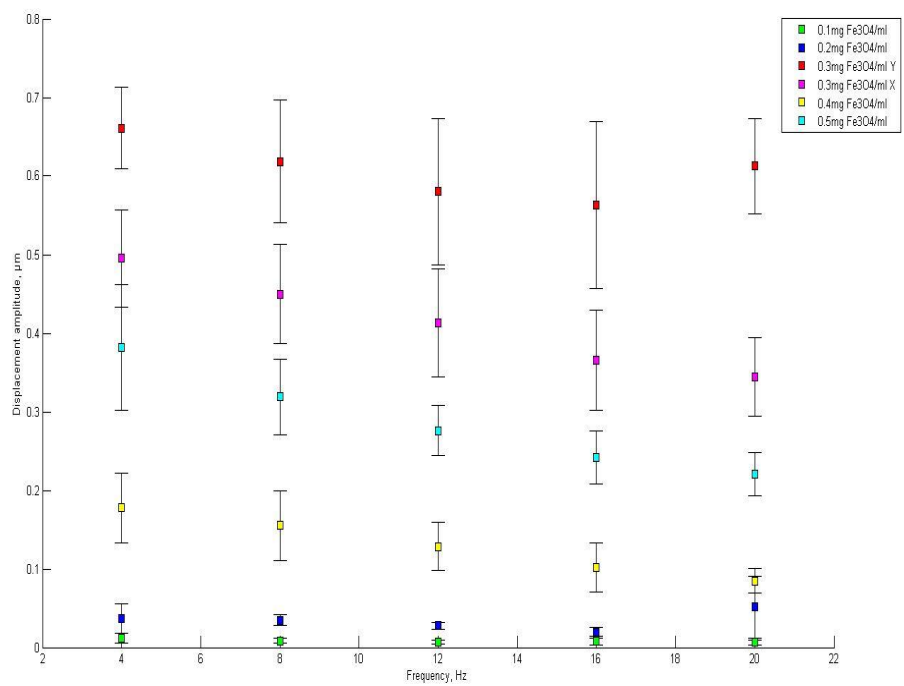


Figure 4.16: Displacement of the inserts at different frequency

4.2 Simulation results

The results shown below are obtained from the simulation done on Comsol software. The results are from both the 2D-axis-symmetric and 3D model.

4.2.1 2D-Axis-symmetric simulation results

All the 2d-axis symmetric results are done with an excitation frequency of 4Hz.

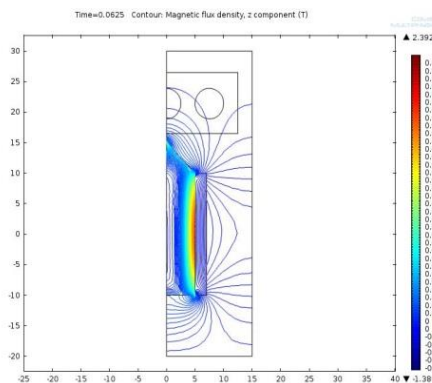


Figure 4.17: Magnetic flux density in the z-component

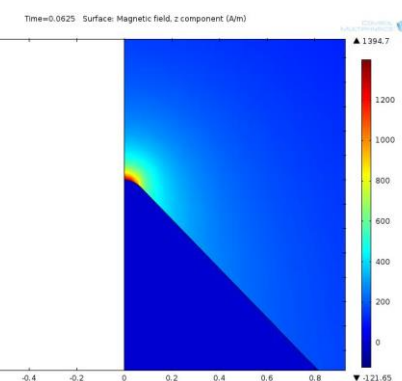


Figure 4.18: The z-component Magnetic field strength at the tip of the iron core

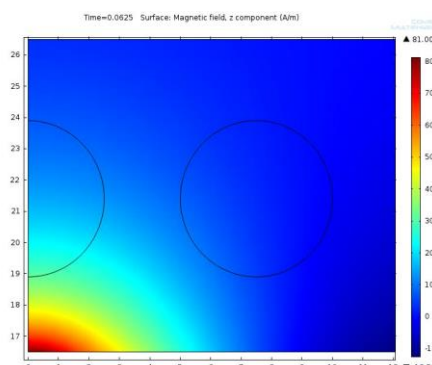


Figure 4.19: The z-component Magnetic field inside the phantom

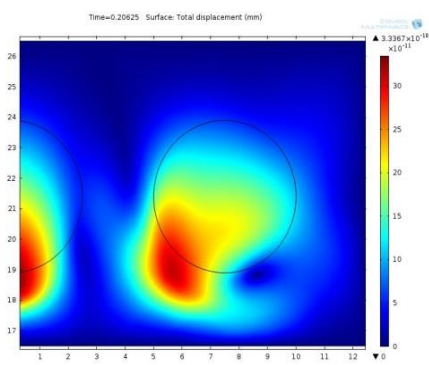


Figure 4.20: Effect of the magnetic force on the inserts and the surrounding

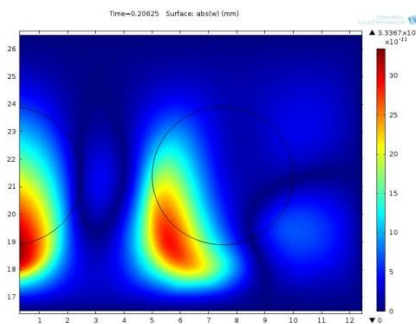


Figure 4.21: z-component displacement of the inserts and the surrounding

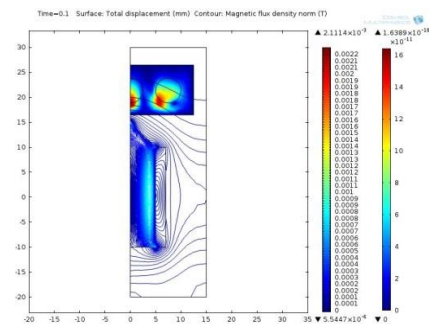


Figure 4.22: Total displacement and Magnetic flux density

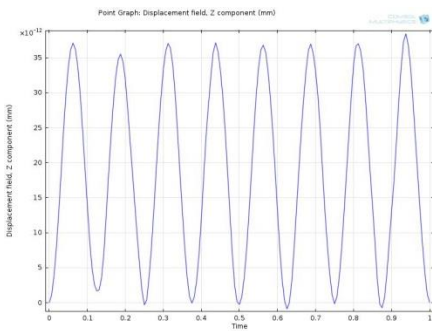


Figure 4.23: Sinusoidal movement of the area in between the inserts

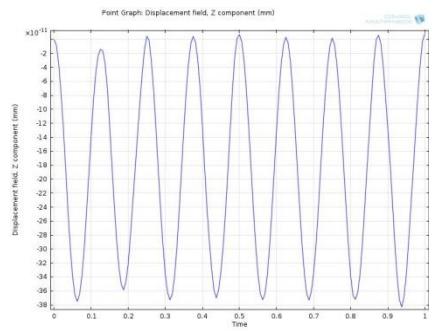


Figure 4.24: Sinusoidal movement of the inserts

4.2.2 3D-simulation results using a 4Hz excitation frequency

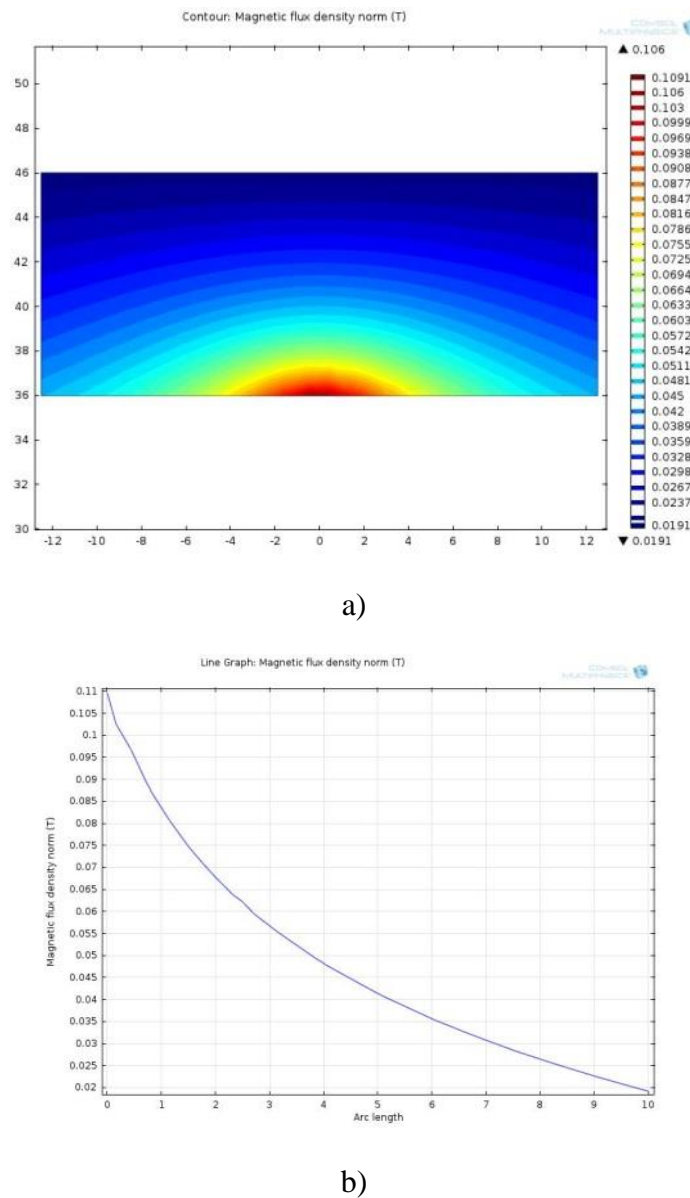
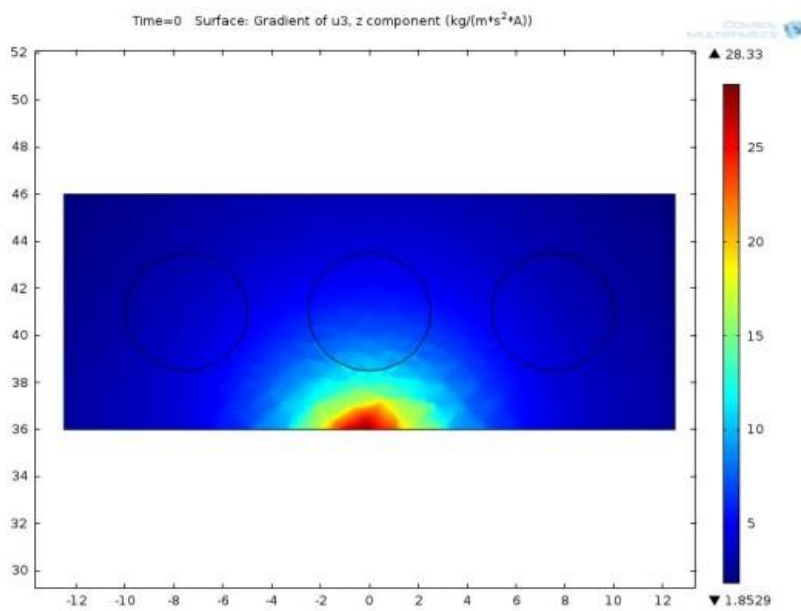
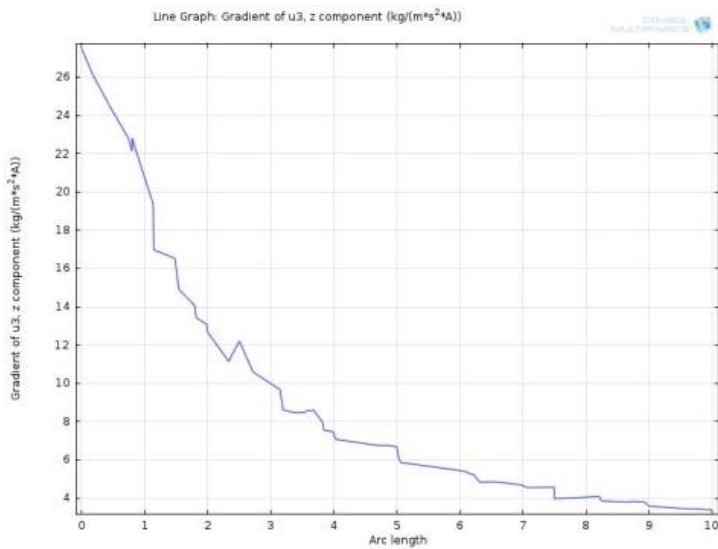


Fig.4.2.2 Simulation results for the magnetic field a) The magnetic flux density norm b) The line graph showing the decrement of the flux density

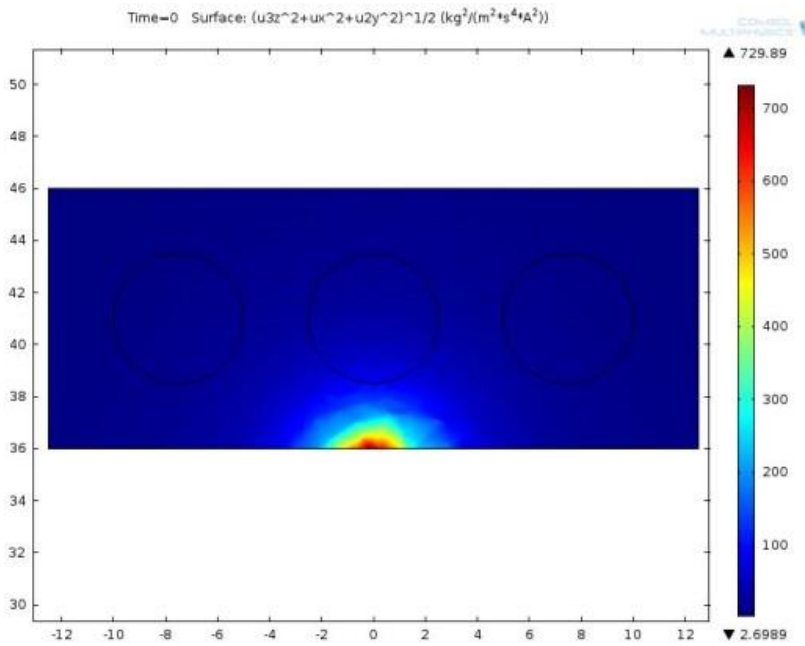


c)

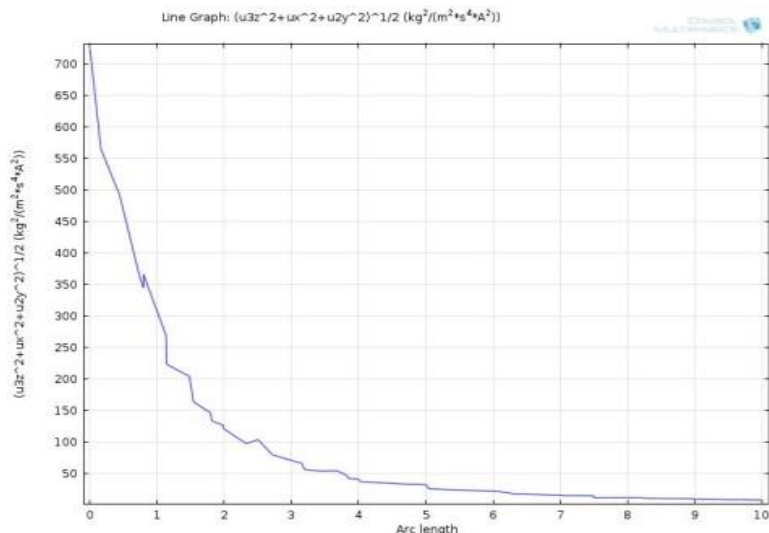


d)

c) z-component magnetic flux gradient d) The z-component gradient line graph

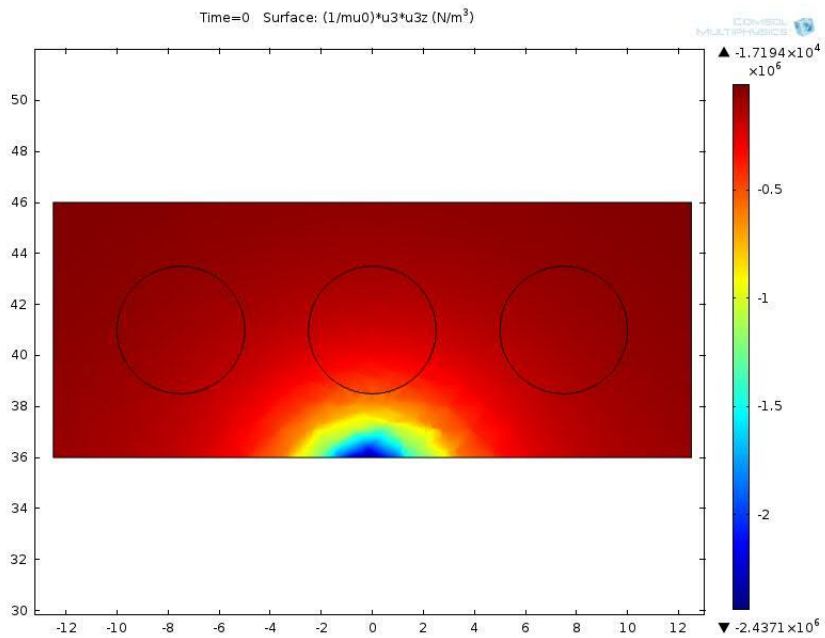


e)

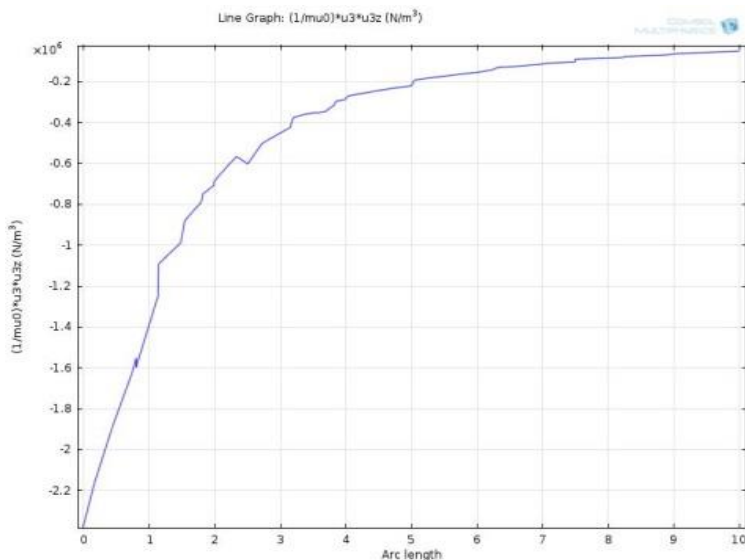


f)

- e) The field gradient norm in all directions f) line graph representing field gradient norm in all directions

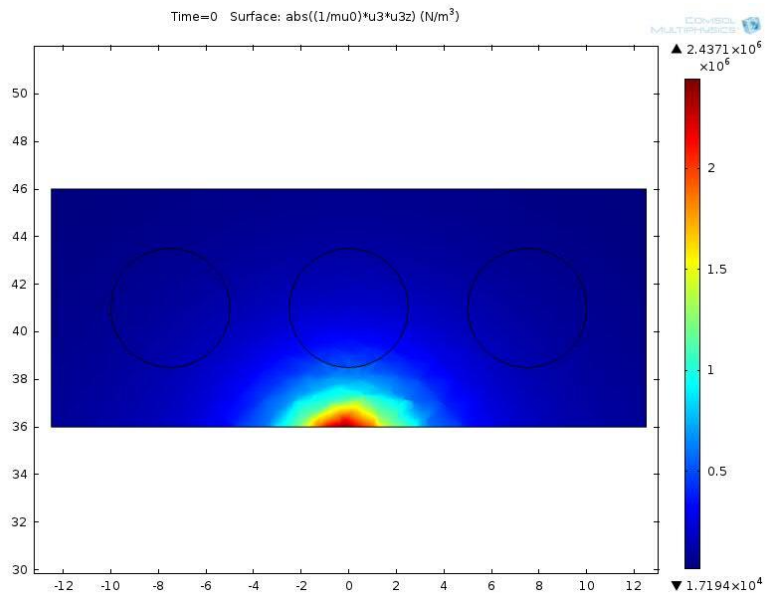


g)

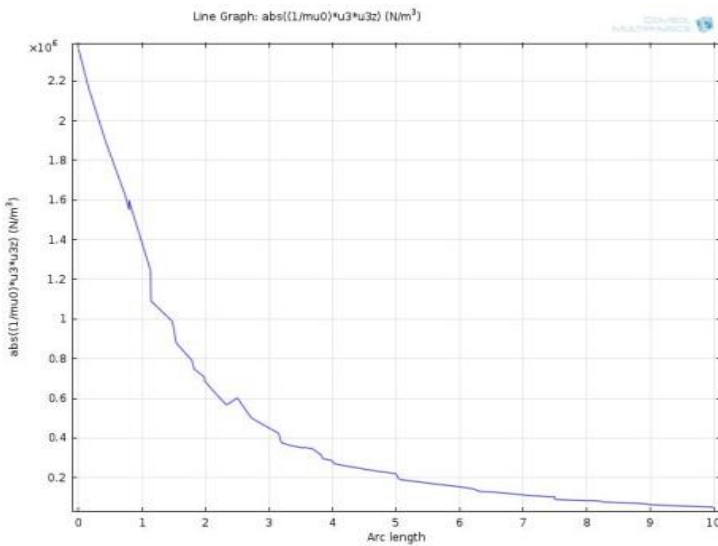


h)

g) The magnetic force per volume h) The line plot for the magnetic force per volume

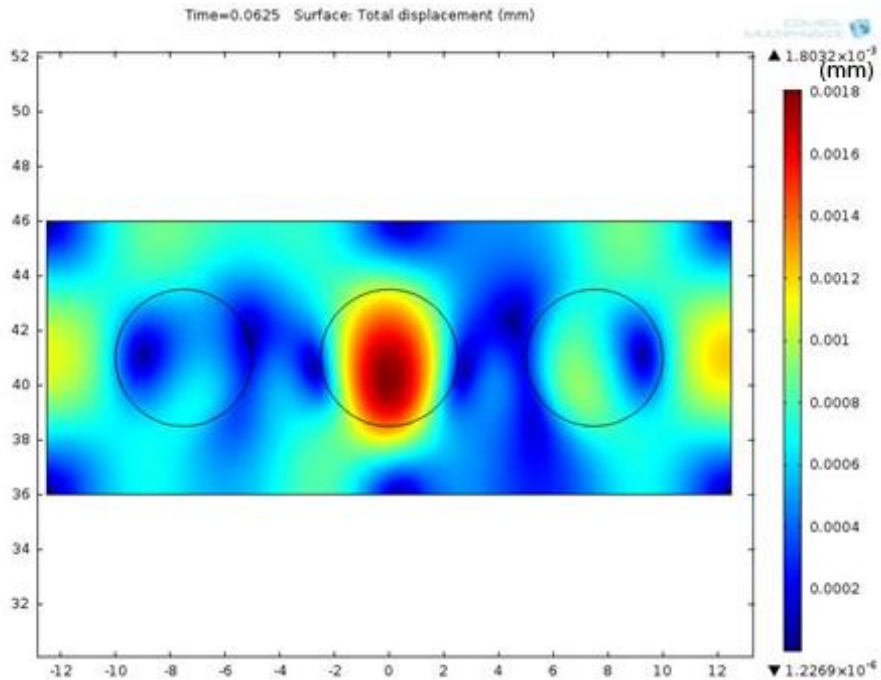


i)

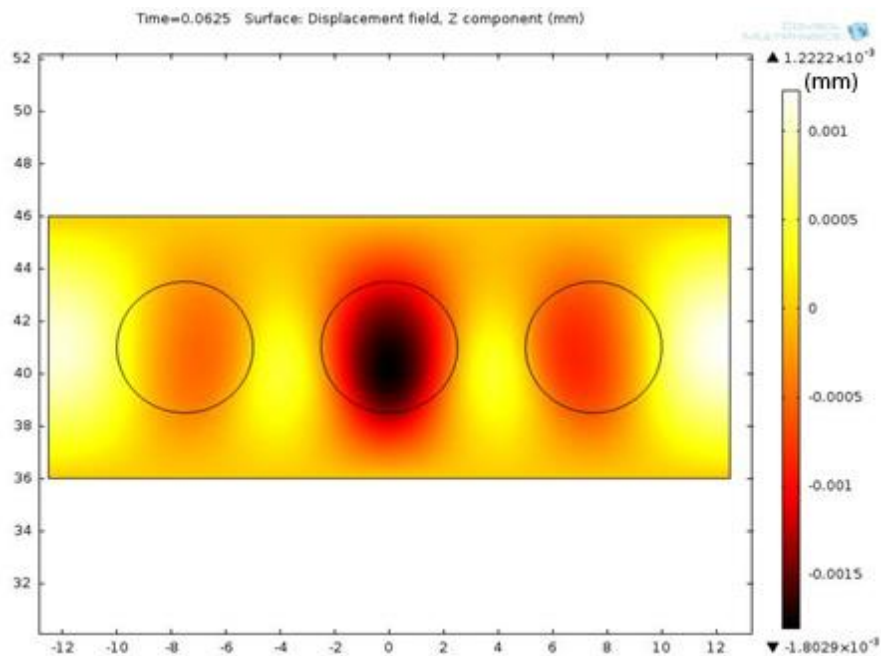


j)

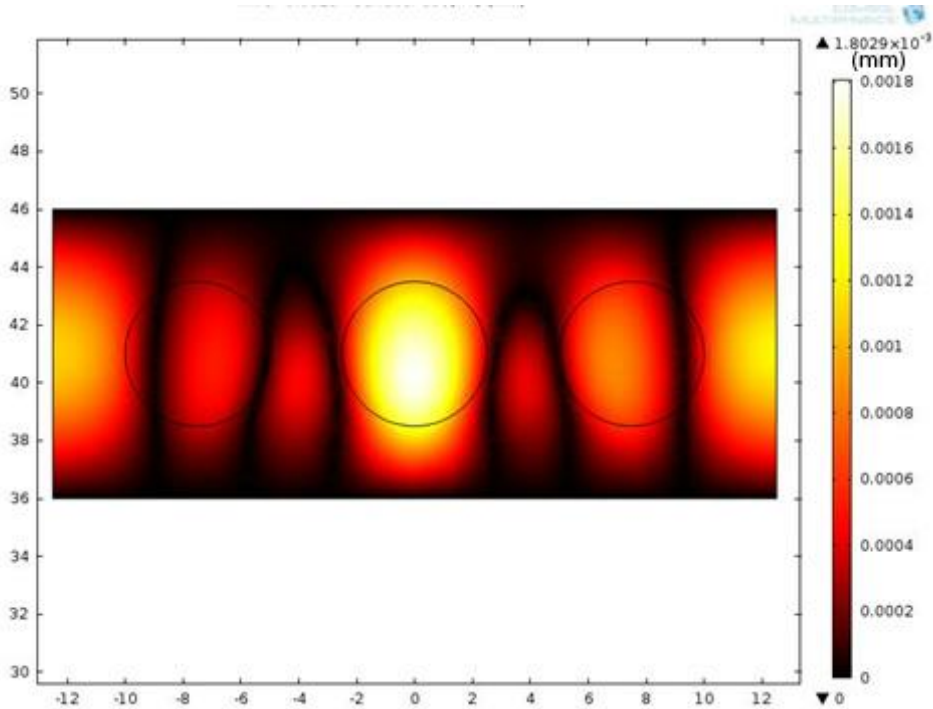
- i) The absolute value of the force per volume j) The corresponding line graph



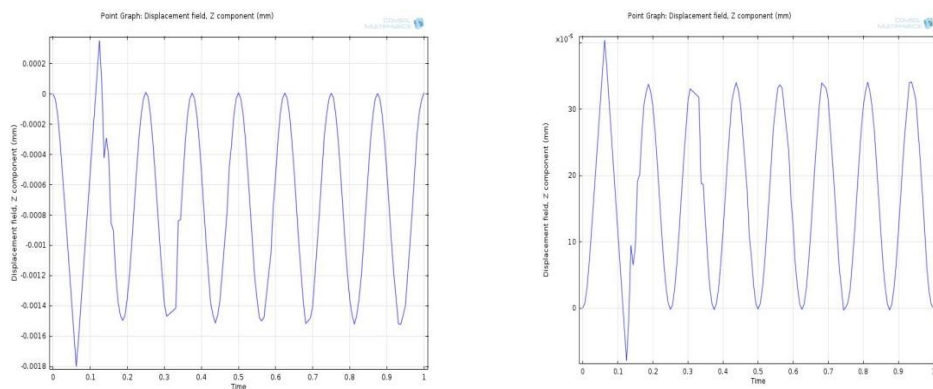
k) Total displacement of the entire area in millimeter



l) The z-component displacement in millimeter



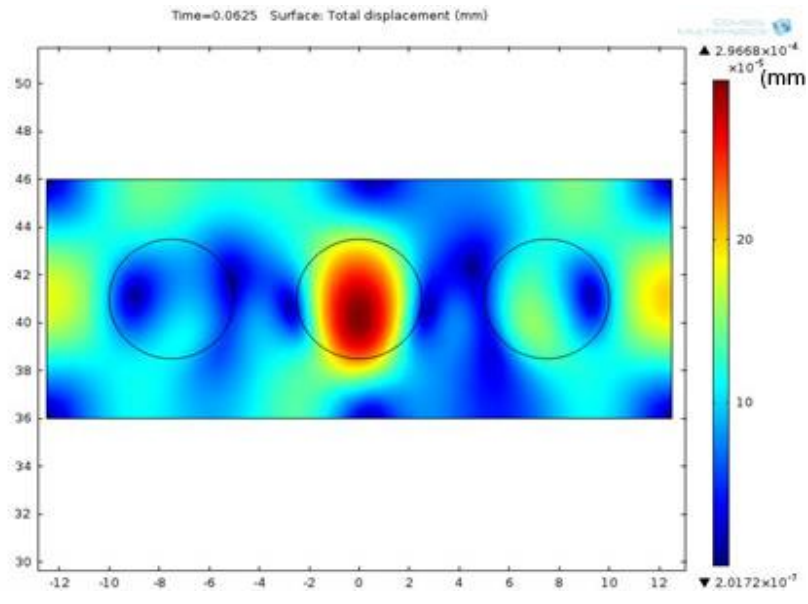
m) Absolute value of the the z-component displacement in millimeter



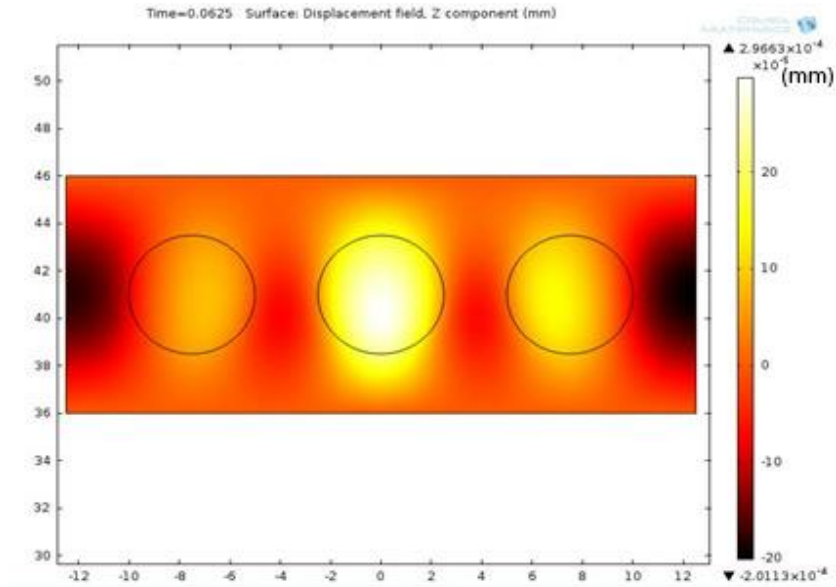
n) Sinusoidal movement of the area in between the inserts

o) Sinusoidal movement inside the inserts

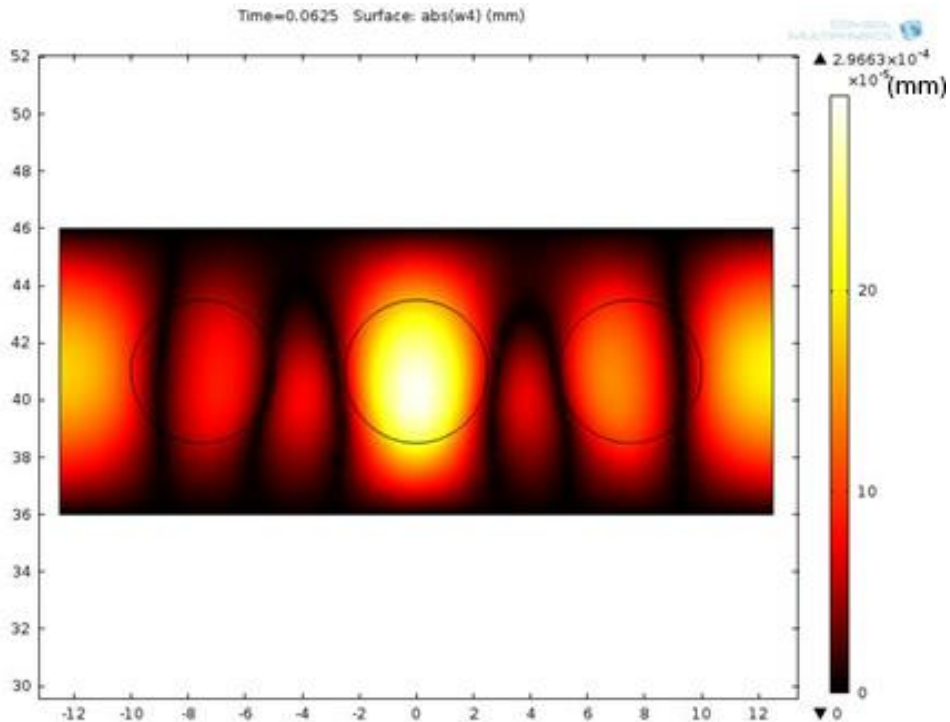
4.2.3 3D-simulation results using a 8Hz excitation frequency



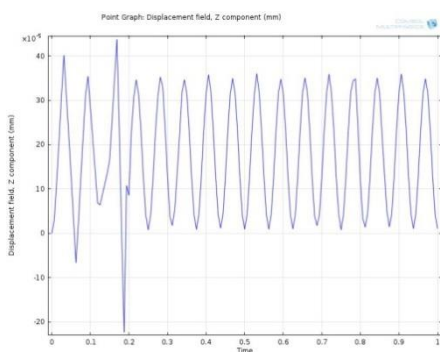
a)



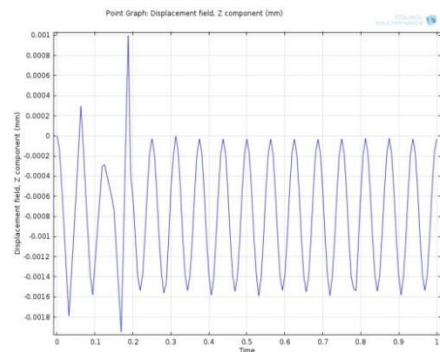
b)



c)



d)



e)

Fig 5.2.3; Motions inside the tissue mimicking phantom a) total displacement of the entire area b) the vertical or z-component displacement c) the absolute value of the vertical displacement d) sinusoidal motion inside the insert e) sinusoidal motion in between the insert

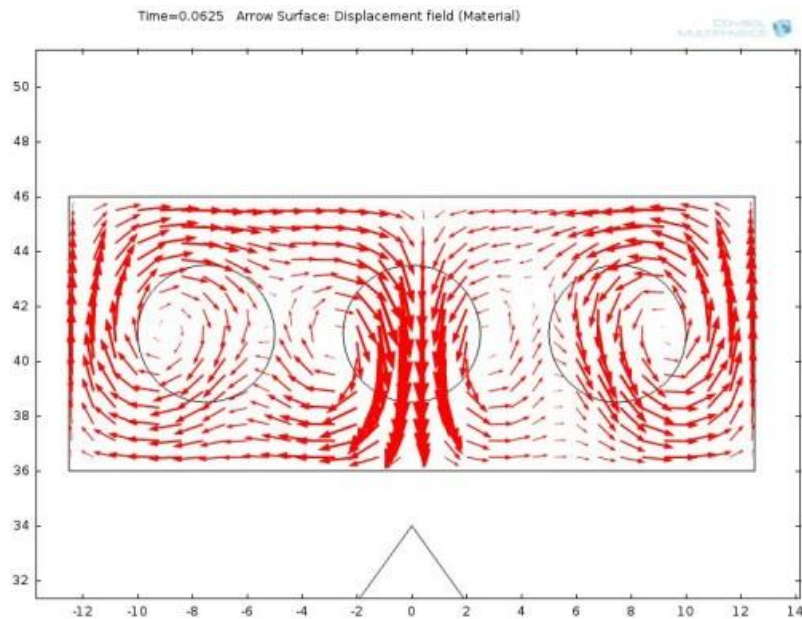


Figure (X): Arrow surface showing motion displacement of the entire area

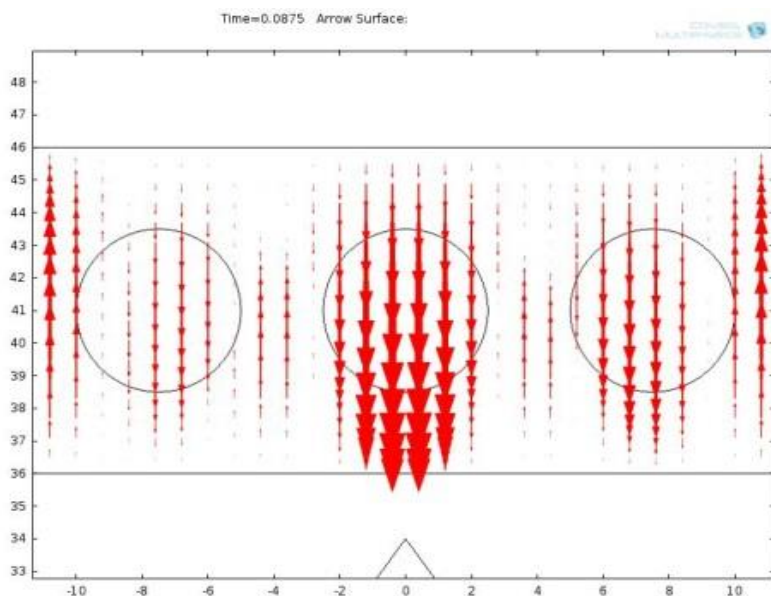


Figure (Y): Arrow surface z-component displacement

5, Discussions

5.1 Experimental results

The following discussions are based on the experimental results from both the high and low concentration set up explained in the material and methods section, on the measurements of the motion detection and localization of magnetic nanoparticles labeled inside a tissue mimicking phantom using the technique Magneto-motive ultrasound (MMUS) imaging.

As it can be seen from the images displayed on fig.4.1 and fig.4.9, the iron (III) oxide Fe_3O_4 concentration of the inserts are different for the inserts labeled on the other side of the 0.3mg/ml of Fe_3O_4 concentration. This is done to see which one would give higher displacement of the inserts and the area in between the inserts. It can be seen from table 2 and table 3 that the average displacements obtained for the high concentration set up is greater than from the low concentration set up, except for the 0.3mg/ml of Fe_3O_4 . However, the 0.3mg/ml of Fe_3O_4 concentration which is labeled in the center in both set ups, shows a smaller displacement for the high concentration set up than the low concentration, and this is because in the low concentration set up as the 0.2mg/ml of Fe_3O_4 and 0.1mg/ml of Fe_3O_4 inserts cannot be attracted high enough to the field gradient due to their low concentration, their movements become less, and this will give the 0.3mg/ml of Fe_3O_4 insert to move freely and dominate the other inserts labeled on the side. But in the high concentration set up, even though the 0.4mg/ml of Fe_3O_4 and 0.5mg/ml of Fe_3O_4 are a bit far from the high field gradient, which is much closer to the 0.3mg/ml of Fe_3O_4 insert, their high concentrations play a great role in making them displace more compared to the 0.2mg/ml and 0.1mg/ml of Fe_3O_4 in the low concentration set up.

Fig.4.2 and fig.4.10 show the displacement of the insert and the surrounding at all ranges of frequencies 0-50Hz; here it can be seen that the movement of the inserts are a bit hidden. That is because other movements from the transducer, noise and from the set up itself (having different frequencies) dominate the entire motion. However, after having

excluded all the other frequencies, we are left with the motion of the insert and the area in between which is moving at a frequency of 8Hz as depicted in fig 4.3 and fig 4.11 for the high and low concentration, respectively.

The movement of the inserts are in phase with each other as they are all attracted to the field at the same time but here the amplitudes of the movement are different for the different inserts as showed in table 2 and 3 for two possible reasons; the first could be the location of the inserts, that is the field gradient decreases with distance away from the tip of the core which makes the insert move with different amplitudes. The second could be the difference in concentration of the inserts; the higher the iron concentration of the insert has, the more it gets attracted, which in turn would cause the insert to have a higher displacement. When the inserts are attracted to the field, the region between those inserts goes in opposite direction and this shows that the motion of the area in between is more or less out of phase with the movement of the inserts, which proves the hypothesis we started with; mechanical reflection of the conservation of mass within the phantom volume as depicted in fig.4.4 and fig.4.12. The value of the displacements in table 2 and 3 shows for the different cross-sections and it appears to be different and that could be due to inhomogeneity of the iron (III) oxide in the inserts.

As it can be seen on fig.4.5 and fig.4.6, the phase of the inserts and the area in between are π radian out of phase. This is because when the magnetic field is turned on the magnetic nanoparticles start to get attracted towards the field gradient due to their magnetic nature, then in turn the area in between goes in opposite direction. This could also be seen from the viscoelastic nature of the material in which the inserts are embedded as explained in the material section.

From the pictures above on fig. 4.8 and fig. 4.14, it can be seen that, the movements of the area in between are excluded to clearly see the vertical displacements of the inserts, moving at a frequency of 8Hz. This shows effectively the use of algorithm made by Maria Evertsson et al [28].

The graph in fig. 4.15 shows the displacement for the different concentration of the inserts. The vertical and the horizontal axes represent

the displacement and concentration respectively. Considering the red marked point, the three inserts are given different concentrations: 0.1, 0.2 and 0.3 mg/ml of Fe_3O_4 . Here the experimentation is done at a frequency of 4Hz. As it is seen on the graph, the displacement of the inserts is pretty much proportional to the concentration of the inserts. The insert having the highest concentration, in this case the 0.3mg/ml of Fe_3O_4 , is displaced more than the other two inserts. For this, two explanations could be given; One is that the insert is just above the core and this would help it to acquire sufficient force needed to displace it more and the other could be the concentration, which is large enough compared to the other two inserts on the sides. As explained in the Material and Methods section, the 0.1 and 0.2 mg/ml of Fe_3O_4 inserts are located at equal distance beside of the 0.3mg/ml of Fe_3O_4 insert and also their location from the core is the same. Here these two inserts have different displacement, although they are placed at equal distance from the core and that is because of their different concentration of the Fe_3O_4 . This shows the displacement dependence of the concentration. In the high concentration set up experiment, shown here by the blue marked line, it is observed that the two replaced inserts (0.4mg/ml and 0.5mg/ml of iron (III) oxide) are displaced more than the first two inserts, 0.1 and 0.2 mg/ml. But the middle insert (0.3mg/ml of Fe_3O_4) is displaced less. So here we see that the movement of the middle insert is affected by the other two inserts, and that is because of their tendency to be attracted towards the magnetic field gradient as they have higher concentration compared to the middle insert. Their being attracted makes them displace more which in turn affects the movement of the middle insert to decrease a bit less even though it is placed very close to the high field gradient; this is due to the friction force created between the spacing between the inserts. We could see that the friction force is another factor that affects the displacement of the inserts. Labeling high concentration inserts aside of the middle insert, affects the motion of the middle insert.

As it can be seen from fig.5.16, the displacements of the inserts are taken for the different frequencies used. In general it can be seen for all the concentrations labeled that the displacement is higher when lower frequencies are used; in this case the lowest excitation frequency used is 4Hz. For the rest of the higher frequencies, the displacements become

smaller. However, one explanation could be given for the decrease in displacement while increasing frequency. That is the inverse relationship between the displacement and frequency, keeping that the energy is constant.

5.2 Simulation results of MMUS imaging

5.2.1 2D-axis symmetric

The MMUS imaging technique used the FEMLAB program which is now called Comsol Software to simulate the effects observed on magnetic nanoparticles labeled inside a tissue mimicking phantom up on being exposed to a magnetic field. As explained in the materials and methods section, the simulation was done separately. To see the effects on the magnetic nanoparticles, first we have simulated the magnetic field as shown in fig. 4.17. The figure shows the magnetic flux density in the z -direction, where it emanates from the iron core and extends all the way up inside the phantom. Fig. 4.18 shows the z -component magnetic field strength at a very close look. This magnetic field has a gradient that decreases with distance away from the source.

Fig. 4.19 shows how the z -component of the magnetic field looks like inside the tissue mimicking phantom where the magnetic inserts are labeled. It is seen that there is a decrease in magnetic field strength away from the left corner where the magnetic field enters the phantom. This decrement in strength makes the magnetic force effect on the insert labeled on the side to decrease. This effect is shown on fig. 4.20 and here it shows the total displacement of the inserts and the surrounding. As we are interested in measuring the vertical or in this case the z -directional movement, it is shown in fig. 4.21. The overall picture of the simulation is shown in fig. 4.22, when the magnetic field is coming out at the tip of the iron core, the magnetic inserts start to get attracted towards the highest field gradient. As the magnetic field is time dependent, the inserts show harmonic motion. Looking at movements of different points inside the

insert and in between the inserts, the motions in both regions appear to be sinusoidal and move with a frequency of 8Hz, twice the excitation frequency 4Hz. And also these sinusoidal movements of the inserts and the region in between are π radian out of phase. Fig. 4.23 and fig. 4.24 depicts this phenomenon.

5.2.2 3D-with an excitation frequency of 4Hz

The following images are cross-sectional images of a 3D model. As can be seen from the picture depicted on fig. 4.2.2 a), motion has been induced inside the tissue mimicking phantom due to the magnetic force acting on the magnetic inserts. Here it shows the magnetic flux density norm.

At the start when the magnetic field comes out from the tip of the iron core, it goes through the phantom and extends all the way in all directions to the other ends of the phantom. From the color code it can be seen that the magnetic flux density is highest at the bottom border where the field enters the phantom and decreases all the way up. This is shown by the line plot graph in fig. 4.2.2 b). The plot shows the decrement of the field as it extends from one side of the phantom to the other end. Without the phantom, the magnetic field probably would go further. So here the field decreases more due to the attenuation inside the phantom.

Fig. 4.2.2 c), shows the gradient of the flux density in the z -direction. As can be seen from the color code, the gradient is highest at the bottom surface of the phantom positioned close enough to the tip of the core. The decrement, like the magnetic flux density as it progress through the phantom. The z -component magnetic flux gradient line plot is shown on fig. 4.2.2 d). It shows a step down decrement. Figure 4.2.2 e) shows the norm of the gradient in all the directions x , y and z , and fig. 4.2.2 f) its corresponding line plot, showing the decrement of the gradient in all directions.

The magnetic force or the force per volume is basically proportional to the product of the magnetic flux density and its gradient as to equation (2.10), aside the coefficients. Here figure 4.2.2 g) shows the simulation of the force per volume inside the phantom on the z -direction, and from the color code it can be seen that the force decreases all the way up. Its corresponding line plot is shown on 4.2.2 h). The force is negative as it pulls down the inserts towards the highest field region. So here we are looking at a force as regards magnitude and direction. If we take like -2N/m^3 , it means that the force has a magnitude of 2N in the negative z -direction. For clarification, the absolute value of the z -component force per volume is shown on figure 4.2.2 i), and its corresponding line plot to the right in 4.2.2 J). They both show the decrement of the force as it extends through the phantom from one end to the other.

Upon the exposure of the magnetic nanoparticles and the surrounding to the calculated magnetic force per volume, it is evident from figure 4.2.2 k) that there is motion throughout the phantom and mostly in the magnetic inserts. The color code represents the displacement of the material at different points inside the magnetic inserts and the surrounding, and here the maximum displacement observed is about $1.8\mu\text{m}$ and the minimum is 1.23nm . Due to its location very close to the tip of the core where the magnetic field gradient is highest, the middle insert happens to have displaced more than the other two inserts labeled on the side.

The picture in figure 4.2.2 l) shows the same behavior as in 4.2.2 k), except for the z -component displacement of the entire area. However, as represented by the color code, there happens to be a negative displacement which in this case is for the inserts. Probably, it is because of the inserts being attracted downward in the negative z -direction when first the field is turned on.

The picture depicted on 4.2.2 m) shows the absolute value of the z -component displacement. This is taken just to see the displacement magnitude without the direction. As can be seen from the color code, there seems to be a high displacement in the region between the side inserts and the wall. This is because the phantom is set to slip over the wall, but from

the experimental result depicted in fig. 4.3, the displacement/ motion in the region between the side inserts and the wall seems very small as the phantom is a little bit stuck to the wall of the container.

Considering only the vertical motion/ displacement of the inserts and area in between the inserts, it is seen from figures 4.2.2 n) and 4.2.2 m) that the inserts and the area in between are π out of phase just like the experimental results observed in fig. 5 and 6.

5.2.3 3D with an excitation frequency of 8Hz

Basically, the results obtained using 4Hz as an excitation frequency are the same as those from the 8Hz frequency. The only difference observed is that, using an 8Hz, the inserts and the surrounding area are displaced a factor of 6 less from the results obtained using 4Hz. So from here one could conclude that using higher frequencies as an excitation source, the displacement becomes smaller. From the experimental results on fig. 4.16, we noticed that higher frequency corresponds to smaller displacement and vice versa.

As can be seen from fig. 4.2.2 d and e, motion inside and in between the inserts happens to be sinusoidal just like the results from both the experimental and the simulation (on 2D and 3D at 4Hz). However, here the motion starts with different amplitude, which is expected as the time varying magnetic field was not reached at steady state, but after some time. The movement inside and in between the inserts in all the cases, whether it is experimental or simulation, seems to be π out of phase movement between the magnetic inserts and the area in between. Also the displacement frequency inside the phantom always doubles the excitation frequency used.

The motion of the whole area or total displacement inside the phantom is depicted by the arrow surface on fig. (x), and the corresponding vertical displacement or z-component is displayed on fig. (y). From these two

arrow surface displacements it is seen what happens inside the phantom. As can be seen from the z-component displacement, the magnetic inserts are going down towards the field gradient and the areas in between the inserts, and between the side inserts and the wall go upward away from the magnetic field gradient.

Considering the comparison between the experimental and simulation results, it is observed that the displacements from the experimental results are not the same as the displacements from the simulation. The rationale for this could be the different material property used for the phantom and the inserts for the simulation. That is; the material properties used for the simulation are not fully the same as the experimental: To describe some of the viscoelastic properties used for the simulation, the Young's modulus, the bulk modulus, the shear modulus and the Poisson's ratio take the first place. The only measured value we have from the lab is the Young's modulus (elastic modulus) of the tissue mimicking phantom which is about 830 ± 130 Pa, and this property alone doesn't fully describe the viscoelastic nature of the material. So for the material used in the simulation to describe its viscoelastic nature needs all those material properties mentioned above, though one could be calculated from the other. That being said, we used some values for the Bulk modulus, shear modulus and Poisson's ratio from an article that measured these values for liver tissue. So, to get results more or less the same as the experimental results, and more importantly in displacement wise, having the right material properties and parameter is absolutely necessary. Besides, using the same magnetic field strength, which can be set easily by adjusting the current passing the wrapped coil and the number of coil turns. This project could be extended, in such a way that, by measuring the proper values for the viscoelastic material properties and applying it to the simulation model, would help someone to get the same result as the experiment. Doing so would enhance a proper understanding.

6, Conclusions

In this study, by using the Magneto-motive ultrasound (MMUS) imaging technique, we have managed to do both the experimental and simulation work. We have demonstrated the results from both the experimental and simulation work, and it is seen that the major expected results are the same. The iron oxide inserts labeled inside the phantom happen to move with higher amplitude compared to the area in between the inserts, the inserts and the surrounding move with a frequency of twice the excitation frequency and also it's observed that the motion of the inserts is π out of phase with the area in between the inserts. Once the motion is triggered and attains its steady state. Then ultrasound can be used to image the phenomenon inside the phantom. In this way one would be able to locate the labeled inserts inside the phantom.

7, References

- 1, <http://www.bats.ac.nz/resources/physics.php>
- 2, M. Mehrmohammadi, J. Oh, L. Ma, E. Yantsen. T. Larson, S. Mallii, S. Park, K.P. Johnston, K. Sokolov, T. Milner, and S. Emelianov, “Imaging of Iron Oxide Nanoparticles Using Magneto-Motive Ultrasound”
- 3, M. Mehrmohammadi, Junghwan Oh, Salavat R. Aglyamov, Andrei B. Karpiouk, Stanislav Y. Emelianov “Pulsed Magneto-Acoustic Imaging”
- 4, <http://www.ndk.com/en/sensor/ultrasonic/basic01.html>
- 5, <http://physics.tutorvista.com/waves/longitudinal-waves.html>
- 6, Nicholas J. Giordano, College physics, Volume 1, reasoning and relationships, second edition.
- 7, http://www.visionlearning.com/library/module_viewer.php?mid=102
- 8, <http://physics.tutorvista.com/waves/transverse-waves.html>
- 9,<http://www.ndt-ed.org/EducationResources/CommunityCollege/Ultrasonics/EquipmentTrans/piezotransducers.htm>
- 10, <http://www.yorku.ca/marko/PHYS2211/Lab5.pdf>
- 11, <http://hyperphysics.phy-astr.gsu.edu/hbase/magnetic/elemag.html#c4>
- 12,http://pms.iitk.ernet.in/wiki/index.php/Biot_Savart%27s_Law_and_its_applications
- 13, John F.Schenck “Physical interactions of static magnetic fields with living tissues”
- 14, Elena-Lorena Salabas “Structural and Magnetic Investigations of Magnetic Nanoparticles and Core-shell colloids”

- 15, Jung Hwan Oh, “Magneto-Motive Detection of Nanoparticles and Hemoglobin”
- 16, Diagnostic ultrasound : physics and equipment / [edited by] Peter Hoskins, Kevin Martin, Abigail Th rush. – 2nd ed.
- 17, David Cosgrove, “Ultrasound contrast agents”: An overview
- 18, Nimrod M. Tole, “ Basic physics of ultrasonographic imaging”
- 19,<http://www.ndt-ed.org/EducationResources/CommunityCollege/Ultrasonics/Physics/wavepropagation.htm>
- 20, <http://www.physics247.com/physics-tutorial/ultrasound-physics.shtml>
- 21, <http://www.bats.ac.nz/resources/physics.php>
- 22, Q A Pankhurst, J Connolly, S K Jones, and J Dobson “Applications of magnetic nanoparticles in biomedicine”
- 23, Laura L.Vatta, Ron D. Sanderson, and Klaus R.Koch “Magnetic nanoparticles: properties and potential applications”
- 24, John F. Schenck, “ Safety of Strong, Static Magnetic Fields”
- 25, Jung Hwan Oh, Marc D. Feldman, Jihoon Kim, Hyun Wook Kang, Pramod Sanghi, and Thomas E. Milner “Magneto-Motive Detection of tissue-Based Macrophages by Differential Phase Optical Coherence Tomography”
- 26, Amy L. Oldenburg, Vasilica Crecea, Stephanie A. Rinne, and Stephen A. Boppart “Phase-resolved magnetomotive OCT for imaging nanomolar concentrations of magnetic nanoparticles in tissues”
- 27, Report of the independent Advisory group on non-ionising Radiation “Static Magnetic Fields”

- 28, Maria Evertsson, Magnus Cinthio, Sarah Fredriksson, Fredrik Olsson, Hans W Persson, Tomas Jansson “ Normalization of Magnetic field effects: Towards quantitative Magnetomotive Ultrasound Imaging
- 29, Maria Evertsson, Magnus Cinthio, Sarah Fredriksson, Fredrik Olsson, Hans W Persson, Tomas Jansson “ Frequency and Phase-Sensitive Magnetomotive Ultrasound Imaging of Superparamagnetic Iron Oxide Nanoparticles”
- 30, R . Madru, P. Kjellman, F. Olsson, K. Wingardh, C. Ingvar, F.Stahlberg, J. Olsrud, J. Latt, S. Fredriksson, L. Knutsson, and S. E.Strand, “⁹⁹mTc-labeled superparamagnetic iron oxide nanoparticlesfor multimodality SPECT/MRI of sentinel lymph nodes,” *J. Nucl.Med.*, vol. 53, no. 3, pp. 459–463, 2012.
- 31, M. A. Eghtedari, J. A. Copland, V. L. Popov, N. A. Kotov, M. Motamedi, and A. A. Oraevsky, “Bioconjugated gold nanoparticles as a contrast agent for optoacoustic detection of small tumors,” *Proc. SPIE*, vol. 4960, pp. 76–85, 2003.